

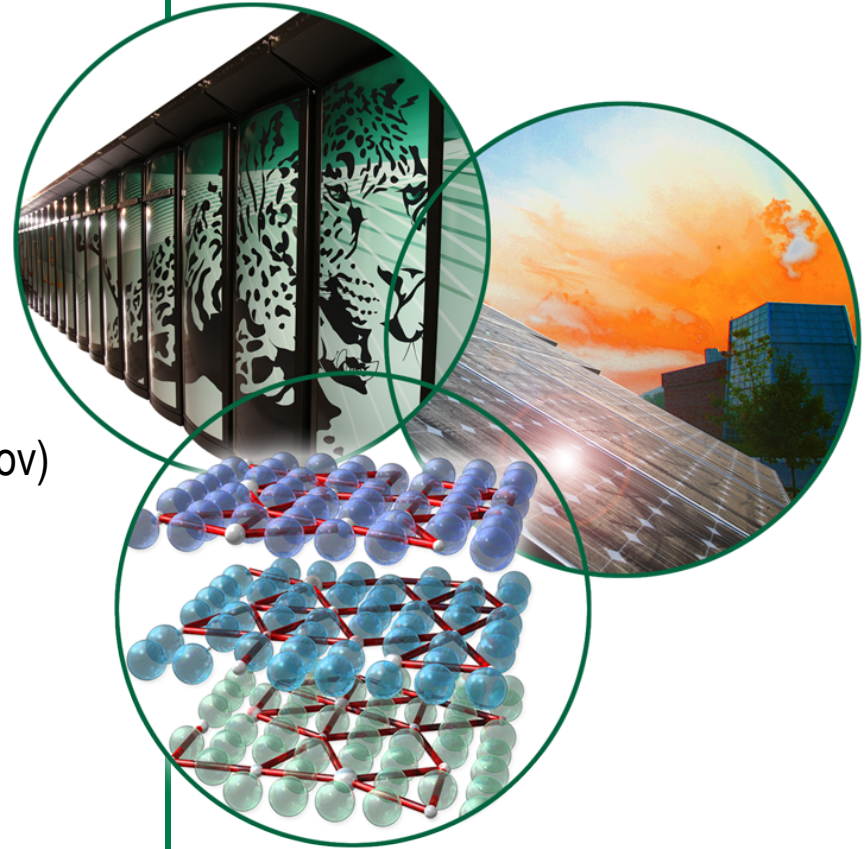
Introduction to Neutron Imaging

Neutron Imaging Team

Hassina Bilheux, Instrument Scientist (bilheuxhn@ornl.gov)
Lakeisha Walker, Scientific Associate
Misun Kang, Ph.D. Student, UTK

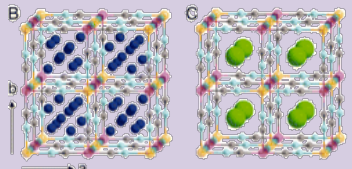
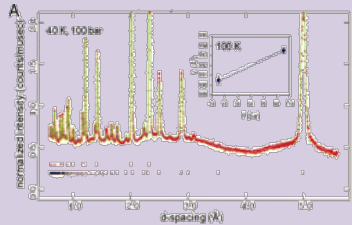
Collaborators (Fluid Flow project):

Ed Perfect and C.-L. Cheng, UTK
J. Warren, ORNL
J. Horita, Texas Tech

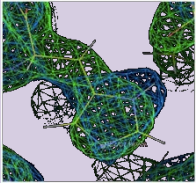


Neutrons Measure Structure

Neutron Diffraction

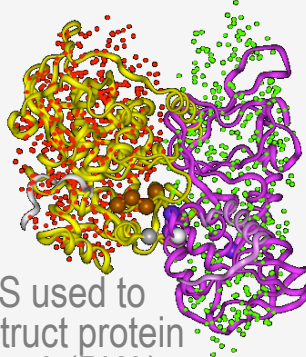


Neutron diffraction of D_2 sorption in $Cu_3[Co(CN)_6]_2$

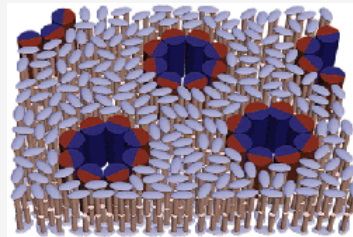


Nuclear and electronic density in enzymes

Neutron Scattering

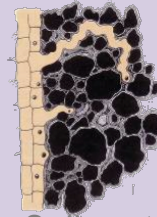


SANS used to construct protein kinase A (PKA)

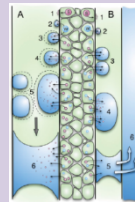


Characterization of biological membranes, colloids, porosity, etc.

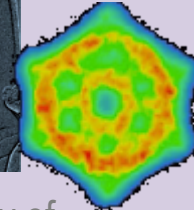
Neutron Microscopy



Soil-root interface (rhizosphere)



Computed tomography



In Vivo Study of Embolism Formation

Neutron Imaging



Fluid interactions in plant-groundwater systems



Ice/water segregation in permafrost structures

Inferred structure (indirect)

Direct structure

10^{-11}

10^{-9}

10^{-7}

10^{-5}

10^{-3}

Dimension (meters)

0.1 Å

1.0 nm

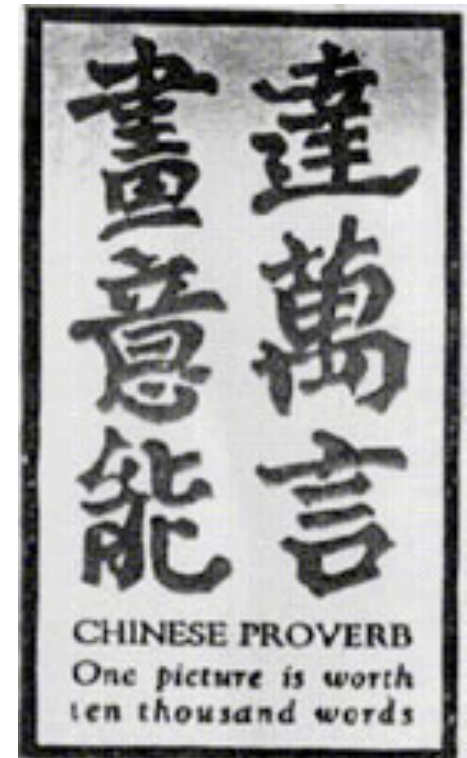
0.1 μm

10.0 μm

1 mm

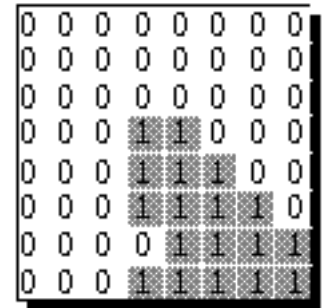
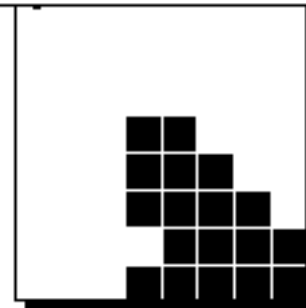
“A picture is worth a thousand words”

- “A good sketch is better than a long speech” (Un bon croquis vaut mieux qu’un long discours) – Napoleon Bonaparte
- Used as advertising in the US in the 1920’s
- Chinese Proverb “A picture is worth *ten* thousand words”



What is imaging?

- **Imaging** is the visual representation of an object: photography, cinematography, medical imaging, X-ray imaging, thermal imaging, molecular imaging, neutron imaging, etc.



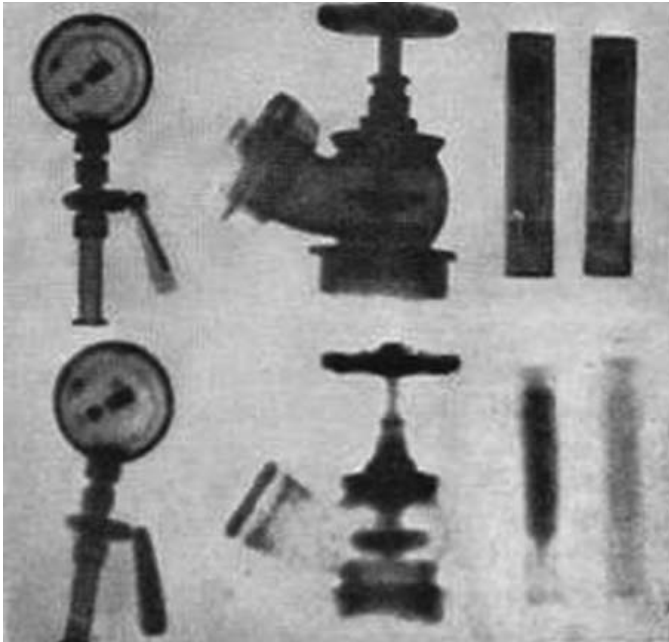
- **Digital Imaging** is a field of computer science covering images that can be stored on a computer as *bit-mapped images*

Imaging throughout Nobel Prize history

- 1901: Roentgen, FIRST Nobel Prize in Physics, **Discovery of X-rays**
- 1979: Cormack and Hounsfield, Nobel Prize in Medicine, **Computed Tomography (CT)**
- 1986: Ruska, Binnig, Rohrer, Nobel Prize in Physics, **Electron Microscopy**
- 2003: Lauterbur and Mansfield, Nobel Prize in Medicine, **Magnetic Resonance Imaging (MRI)**
- 2009: Boyle and Smith, Nobel Prize in Physics, **Imaging semi-conductor circuit, the CCD* sensor**
- (*) Charge-Coupled Device

Early neutron imaging measurements

- Neutron Imaging started in the mid 1930's but only during the past 30 years has it come to the forefront of non-destructive testing



Discovery of neutron in 1932 by Chadwick

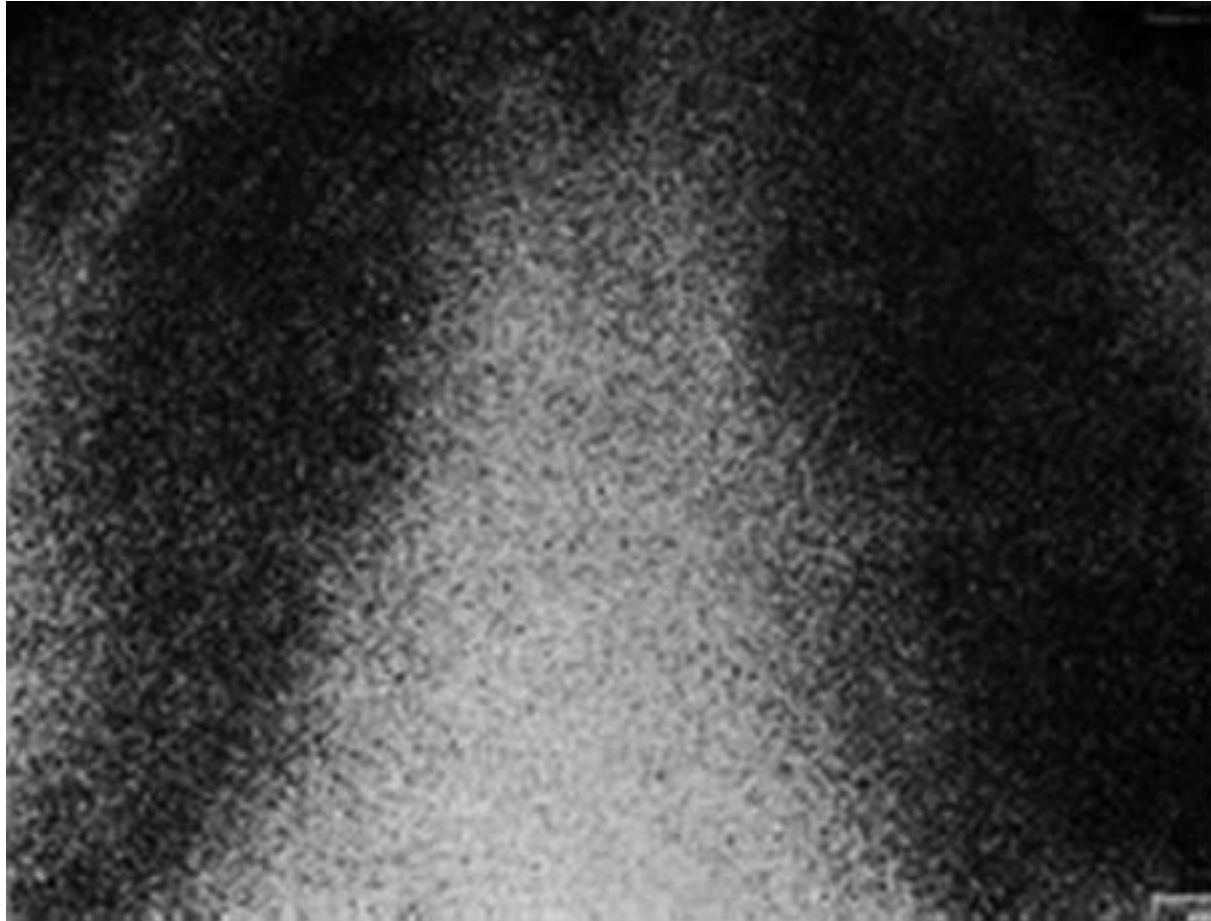
First neutron radiograph in 1935

Left to right: Pressure gauge with metal backplate; fire hydrant and test tubes filled with H₂O and D₂O imaged with gamma-rays (top) and neutrons (bottom)

[Kallman and Kuhn, Research 1, 254 (1947)]

- World class dedicated imaging user facilities such as NIST, PSI, HZB, FRM-II and at many worldwide universities
- World conferences and workshops being held regularly
- Growing worldwide user community

Multiple scattering and low detector spatial resolution

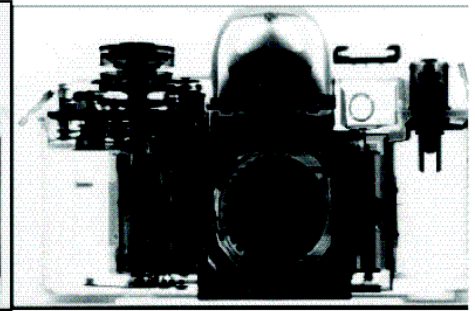
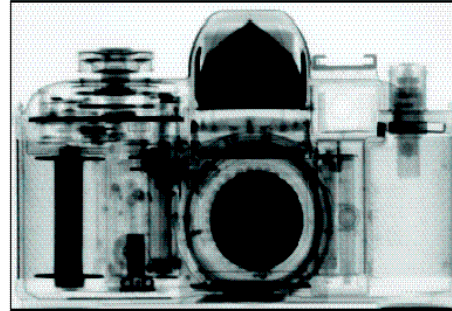


[J. Anderson et al., Br. J. Radiol. 37, 957 (1964)]

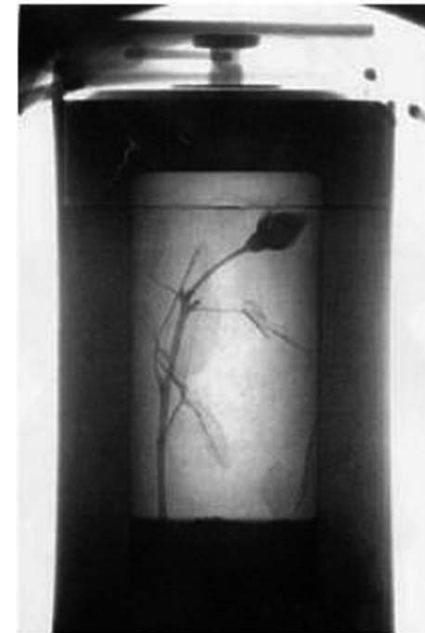
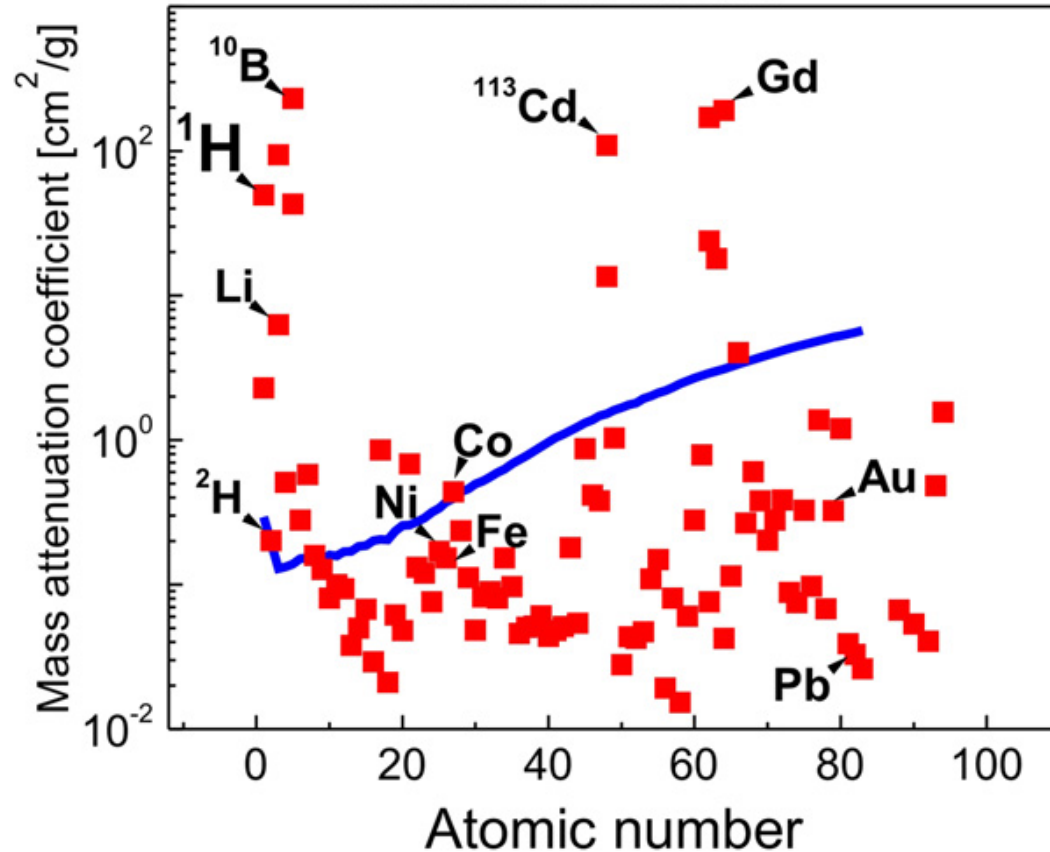
Neutron sensitivity

Neutron Radiograph of camera

X-ray Radiograph of camera



— X-rays (100 keV)
 ■ Thermal neutrons



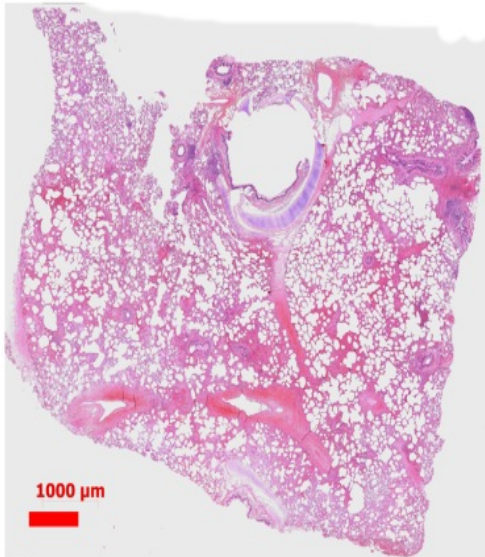
Neutron Radiograph of Rose in Lead Flask

[M. Strobl et al., J. Phys. D: Appl. Phys. 42 (2009) 243001]

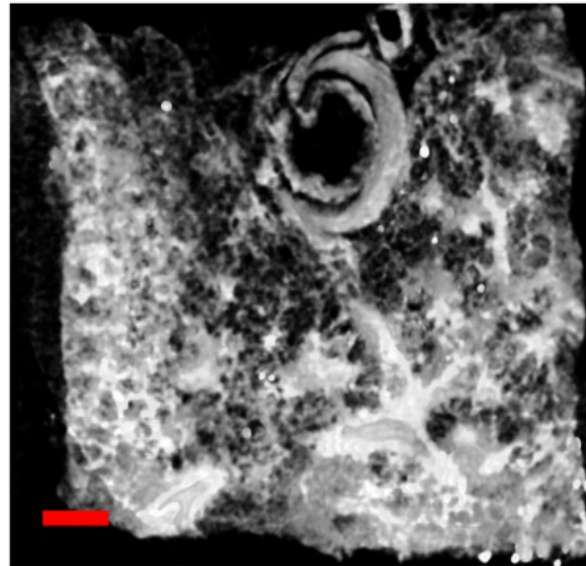
Courtesy of E. Lehmann, PSI

Comparison microscopy/microCT and neutron radiography

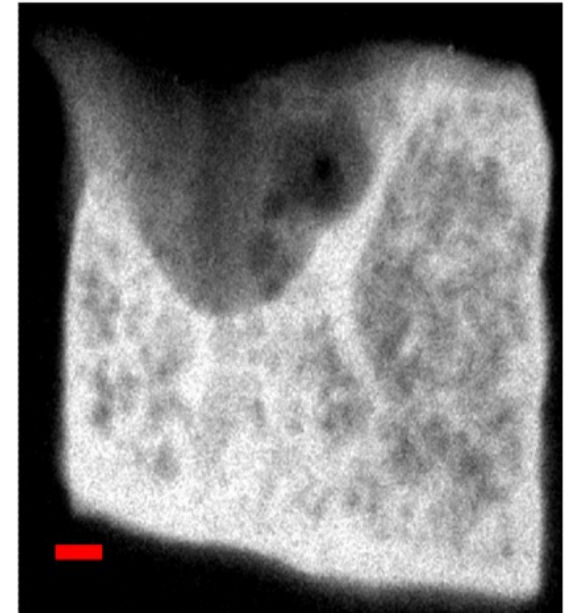
Microscope



microCT

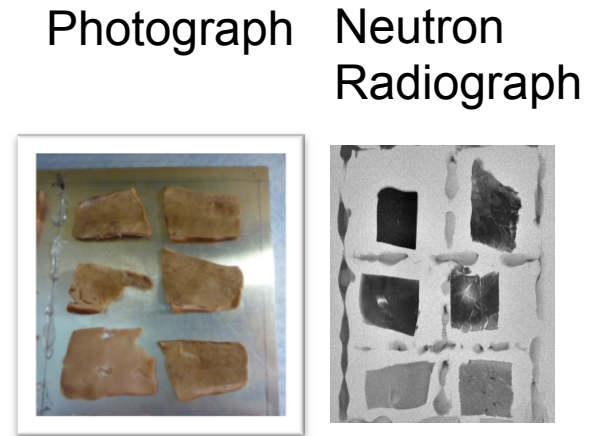
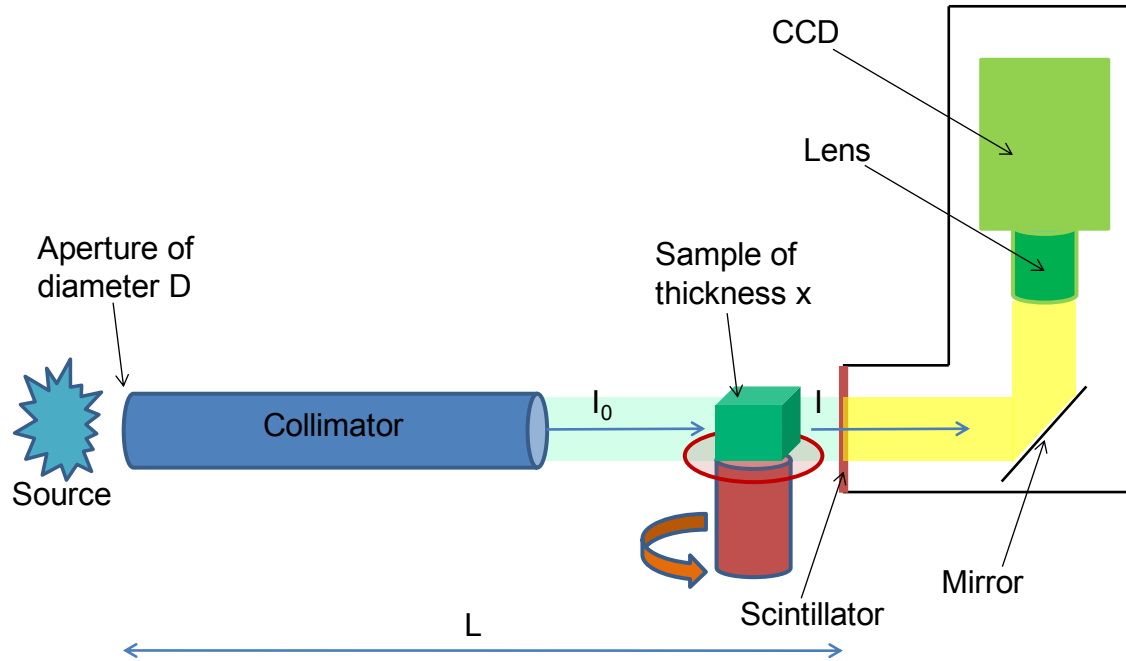


Neutron



- **92% of the pixel intensities agreement between histological and neutron**

Basics of Neutron imaging



Beam attenuation caused by a **homogeneous uniformly** thick sample composed of a **single isotope** is given by

$$I(\lambda) = I_0(\lambda)e^{-\mu(\lambda)x}$$

$$\mu(\lambda) = \sigma_t(\lambda) \frac{\rho N_A}{M}$$

$\sigma_t(\lambda)$ = scattering and absorption

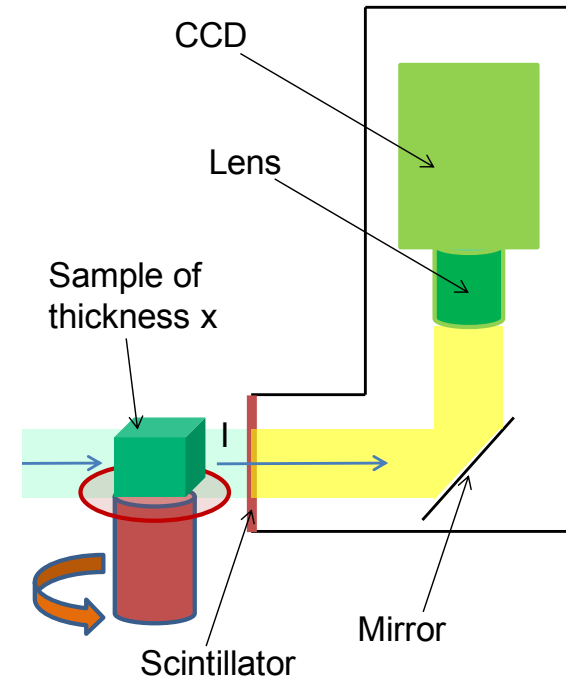
μ is the attenuation coefficient and Δx is the thickness of the sample

$\sigma_t(\lambda)$ is the material's total cross section for neutrons, ρ is its density, N_A is Avogadro's number, and M is the molar mass.

Detection of “imaging” neutrons

- Scintillator-based techniques such as ${}^6\text{Li}(n,\alpha) {}^3\text{H}$
 - Good signal-to-noise (SNR) ratio
 - Large Field Of View (FOV) and 0.01 to hundreds of seconds images
 - BUT spatial resolution limited by the dissipation of particles
 - Can take a lot of neutron flux!

1,1	1,2	1,3	1, ny
2,1	2,2	2,3	2, ny
3,1	3,2	3, ny
..., nx
nx, 1	nx, 2	nx, 3	nx, ny

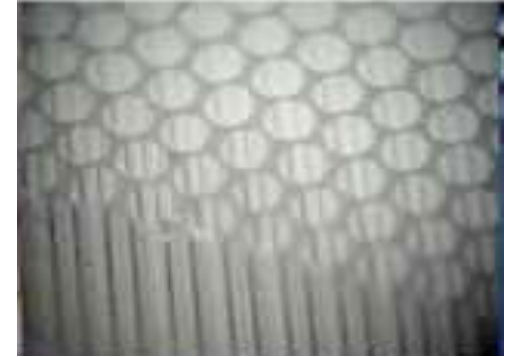


Each pixel is coded using n-bit.
16-bit = pixel value is between 0 and 65535

Detection of “imaging” neutrons (cont’d)

- Pixelated detectors

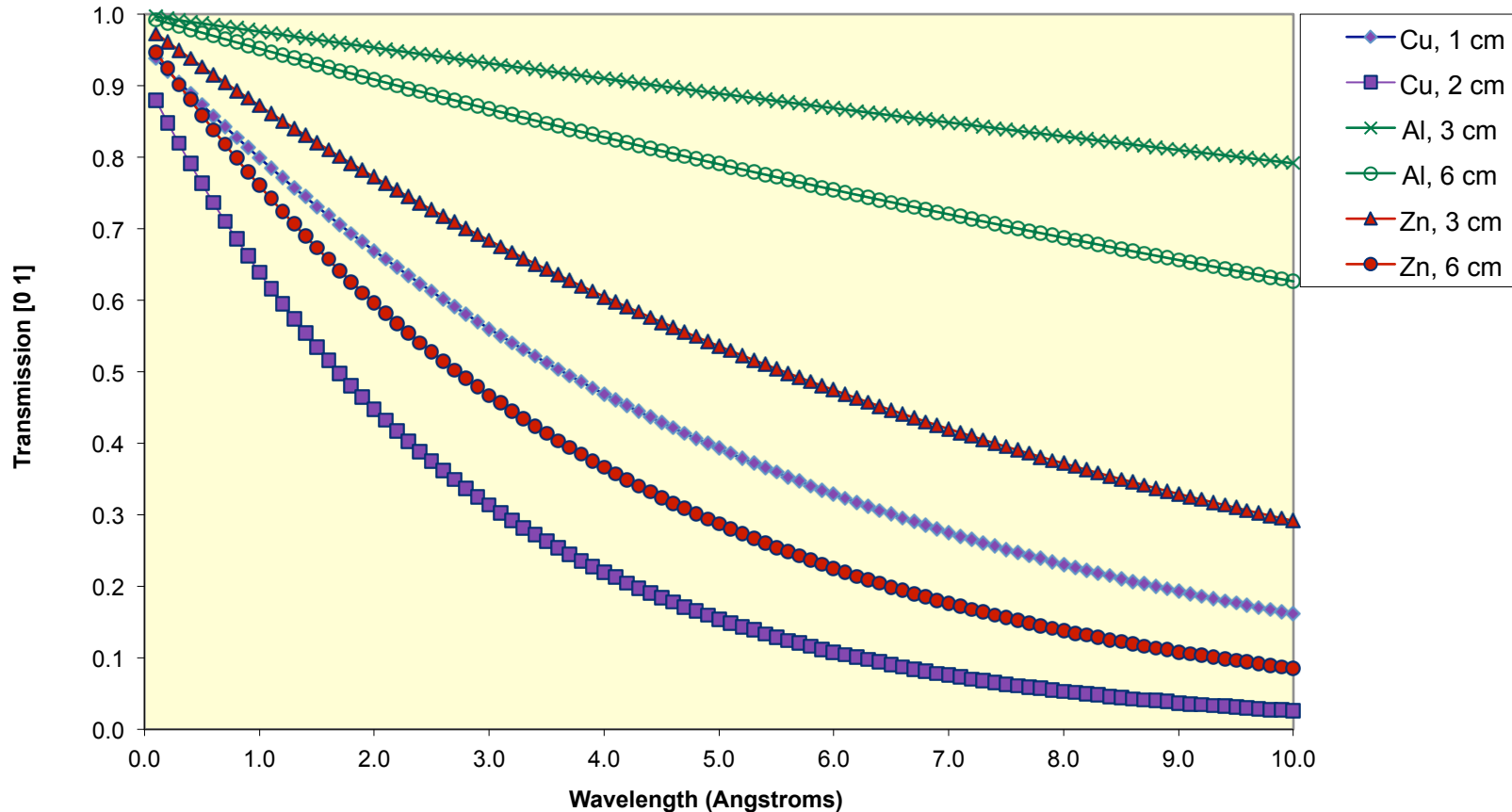
- Micro-Channel Plate (MCP)
- In the direct path of the beam
- Limited FOV for high spatial resolution MCPs
 - 1.4 cm x 1.4 cm at ~ 15 microns
- Encodes events at x, y position and time of arrival, at high temporal resolution ~ 1 MHz
- Detection efficiency has improved for both cold (~70%) and thermal (~50%) energy range
- Absence of readout noise
- Not as gamma sensitive
- Becoming commercial
- BUT: works in relatively low-signal beam!



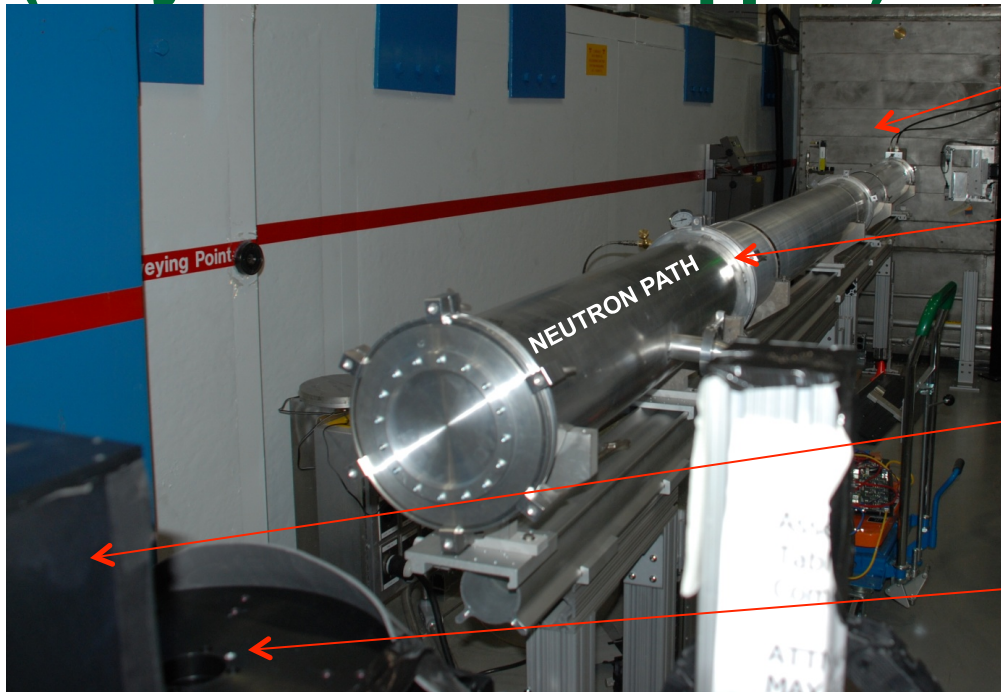
Example: Cu, Zn and Al

Compound	Abs. Coeff. [\AA^{-2}]	Inc. Coeff. [\AA^{-1}]
Cu (100%)	1.78E-09	4.65E-10
Al (100%)	7.75E-11	4.94E-12
Zn (100%)	4.06E-10	5.06E-11

Neutron Transmission through Metals



CG1-D: Neutron Imaging Prototype Beamline (Polychromatic/Chopped)



Chopper Box

He-filled Al flight tubes

Detector housing (CCD, lens, mirror and scintillator)

Sample stage (translation and rotation for neutron Computed Tomography)

HFIR CG1D beamline
Current resolution ~ 50 microns

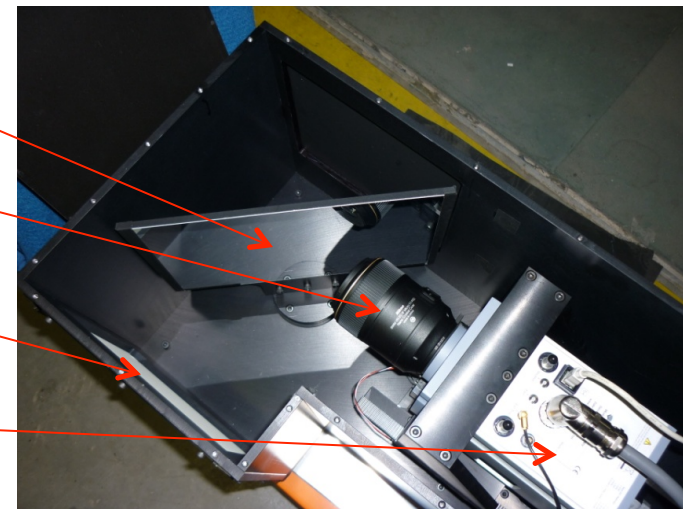
- ANDOR Camera: 4Mpixels – 2048x2048
- Field of view: 7x7cm²
- Quantum Efficiency: 95%

Al Mirror

Lens

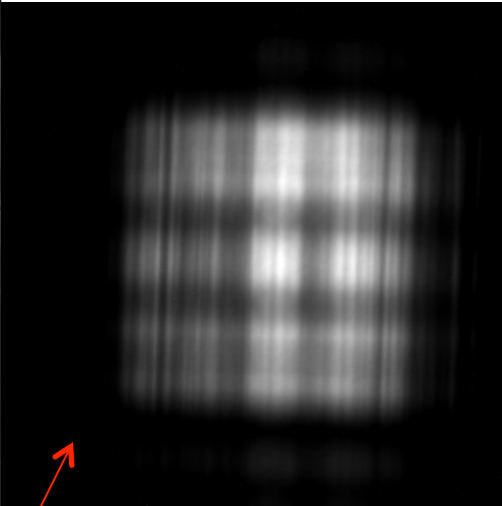
LiF/ZnS scintillator (25 to 200µm thick)

CCD

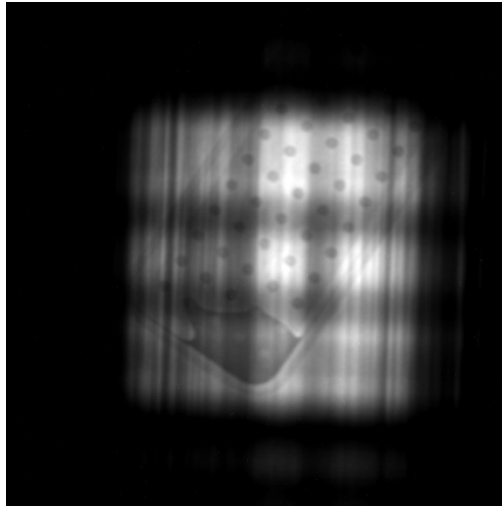


Use of Diffusers

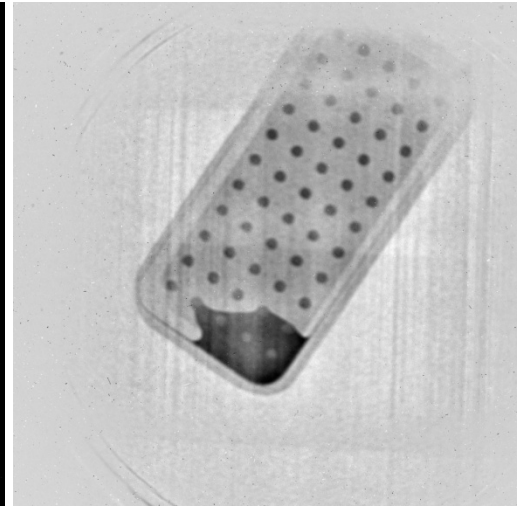
- 1 cm thick Graphite Powder (4 to 10 microns)



Open Beam



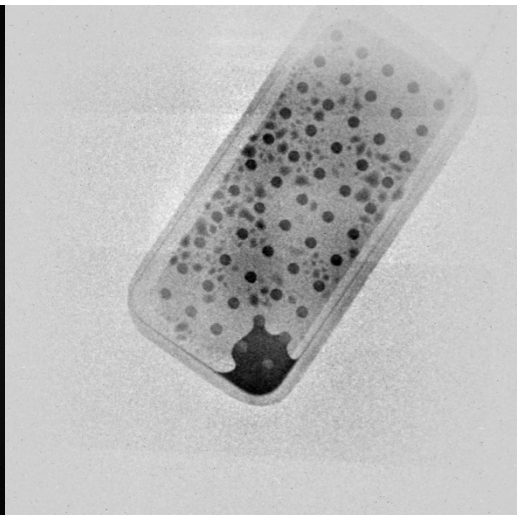
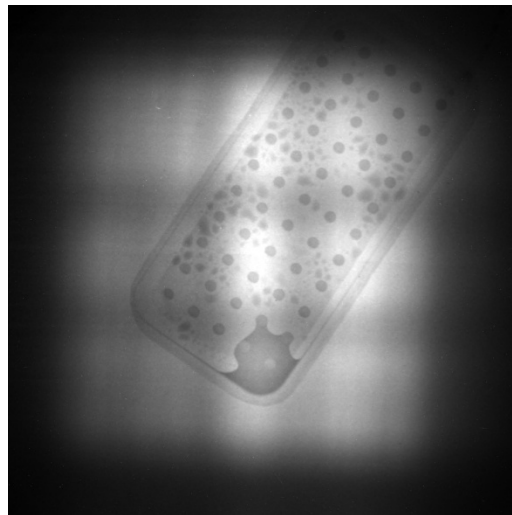
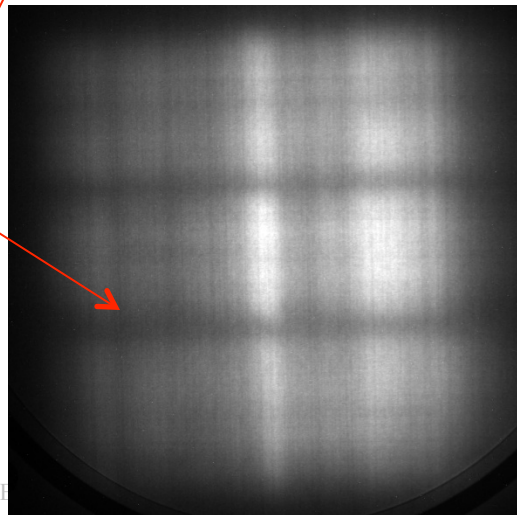
Heat Pipe Sample



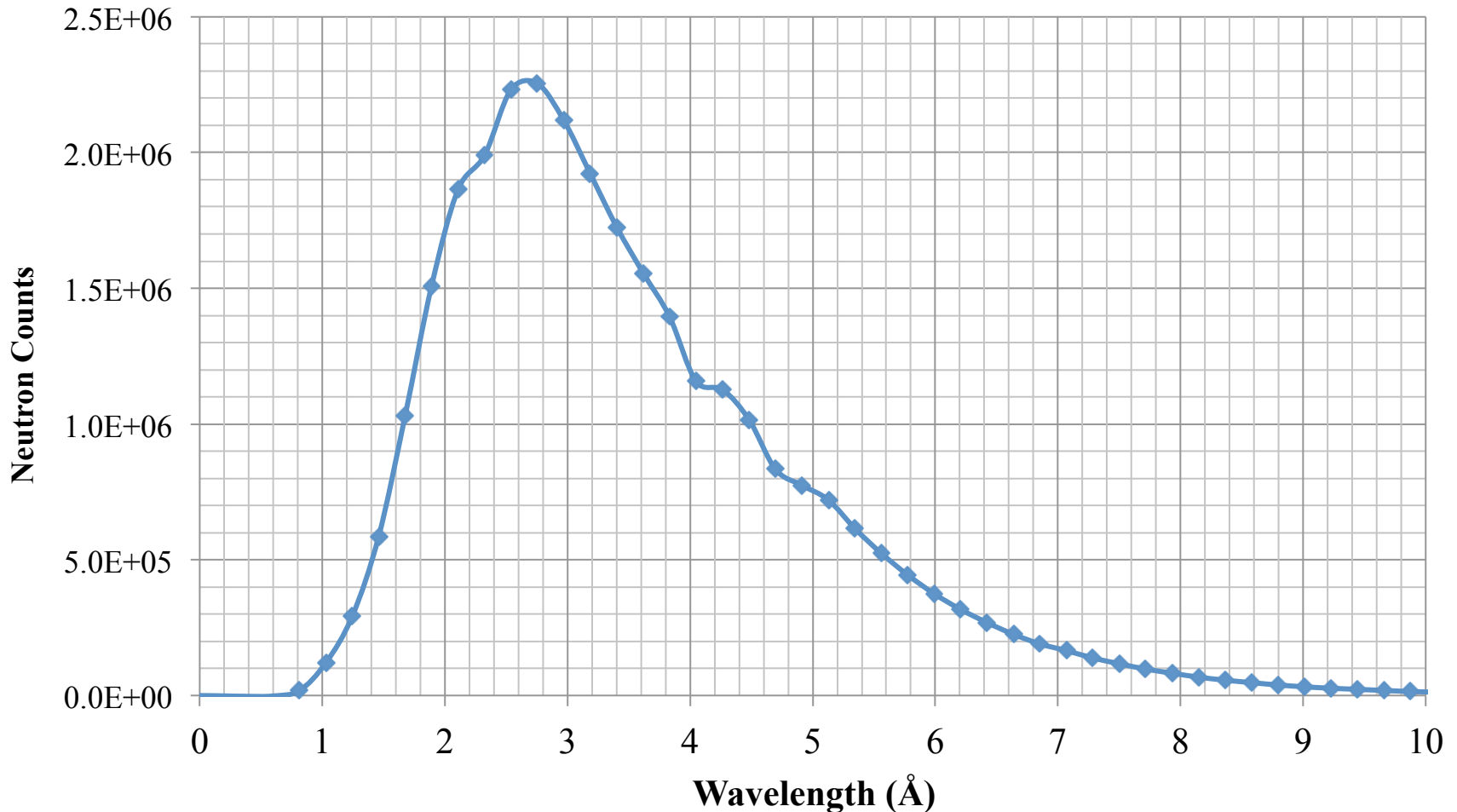
Reduced Image

Without diffuser

With diffuser



CG-1D polychromatic beam

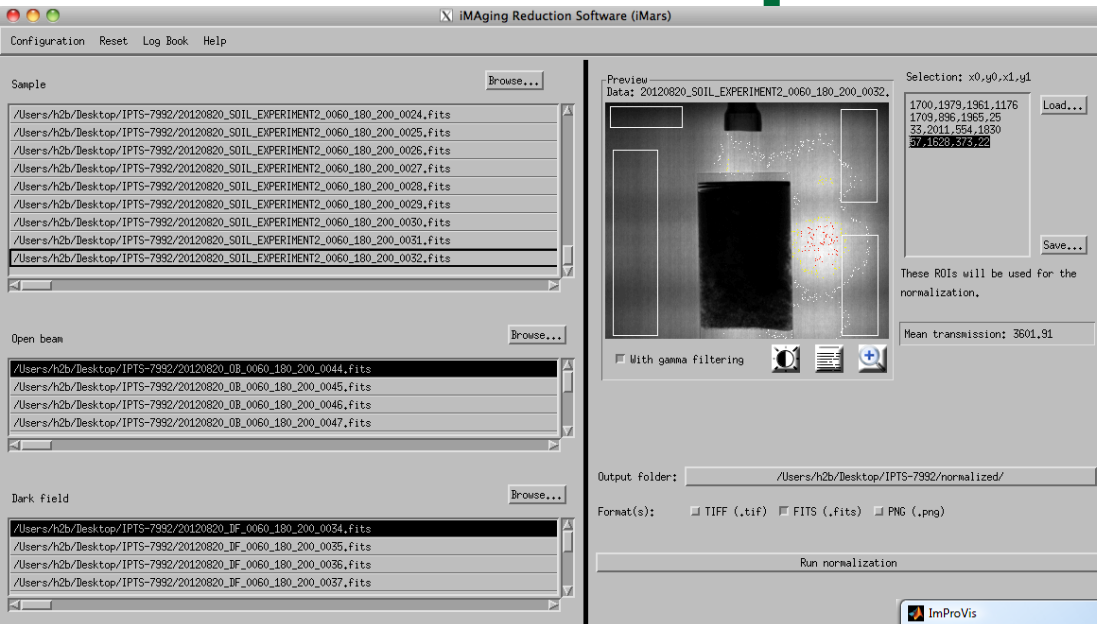


CG-1D spectrum measured with the MCP detector at a flight path distance of approximately 5.5 m, with the chopper running at a frequency 40 Hz and an 5 mm aperture. *[Bilheux et al., ITMNR-7, Canada, June 2012]*

Software Development at CG-1D

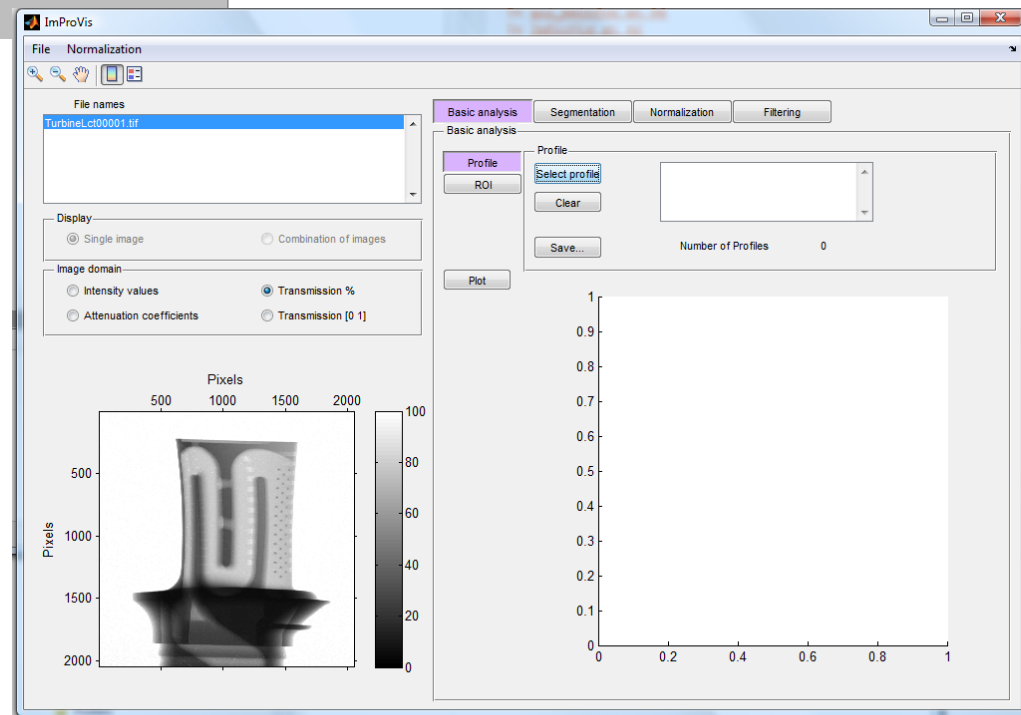
iMARS

(iMaging Reduction Software)
developed J.-C. Bilheux



IMPROVIS

developed by S. Voisin,
M. Kang and H. Bilheux



Conventional Neutron Imaging Techniques at steady-state sources

- Radiography (available at CG-1D)
- Tomography (available at CG-1D)
- Phase Contrast Imaging
- Polarized Neutron Imaging
- Stroboscopic Imaging
- Imaging of processes that happen fast
- Energy selective techniques possible with double-monochromator configuration

Neutron Imaging Techniques at pulsed sources

- **Energy-selective (or Time-of-Flight) imaging**
 - Contrast enhancement
 - Bragg edge
- **Stroboscopic imaging**
 - SNS has a natural clock
- **Neutron Imaging at energies not accessible at reactor facilities**
 - Mainly bio-medical applications

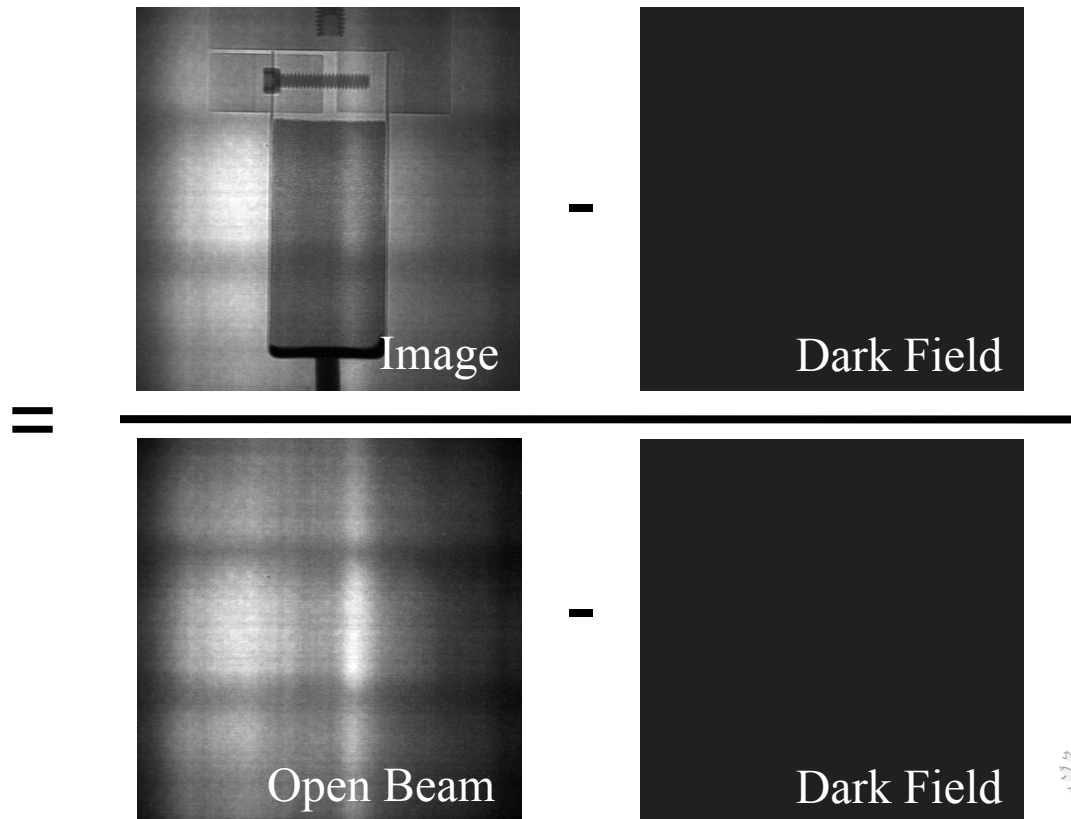
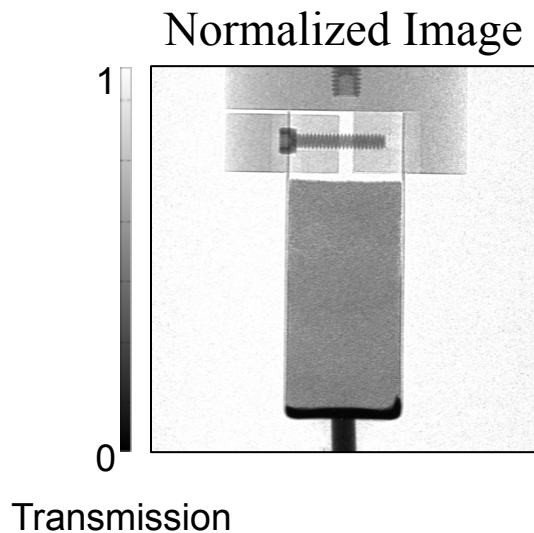
Neutron imaging techniques

- Radiography
- Computed tomography
- Bragg edge imaging
- Neutron phase imaging
- Stroboscopic imaging
- Neutron Stimulated Computed Emission Tomography or NSECT
- Polarized imaging
- Dark field imaging
- Energy resonance imaging

Data Normalization for Imaging

- 2D – Radiography
 - Normalization

$$I_N(i, j) = \frac{I(i, j) - DF(i, j)}{OB(i, j) - DF(i, j)}$$

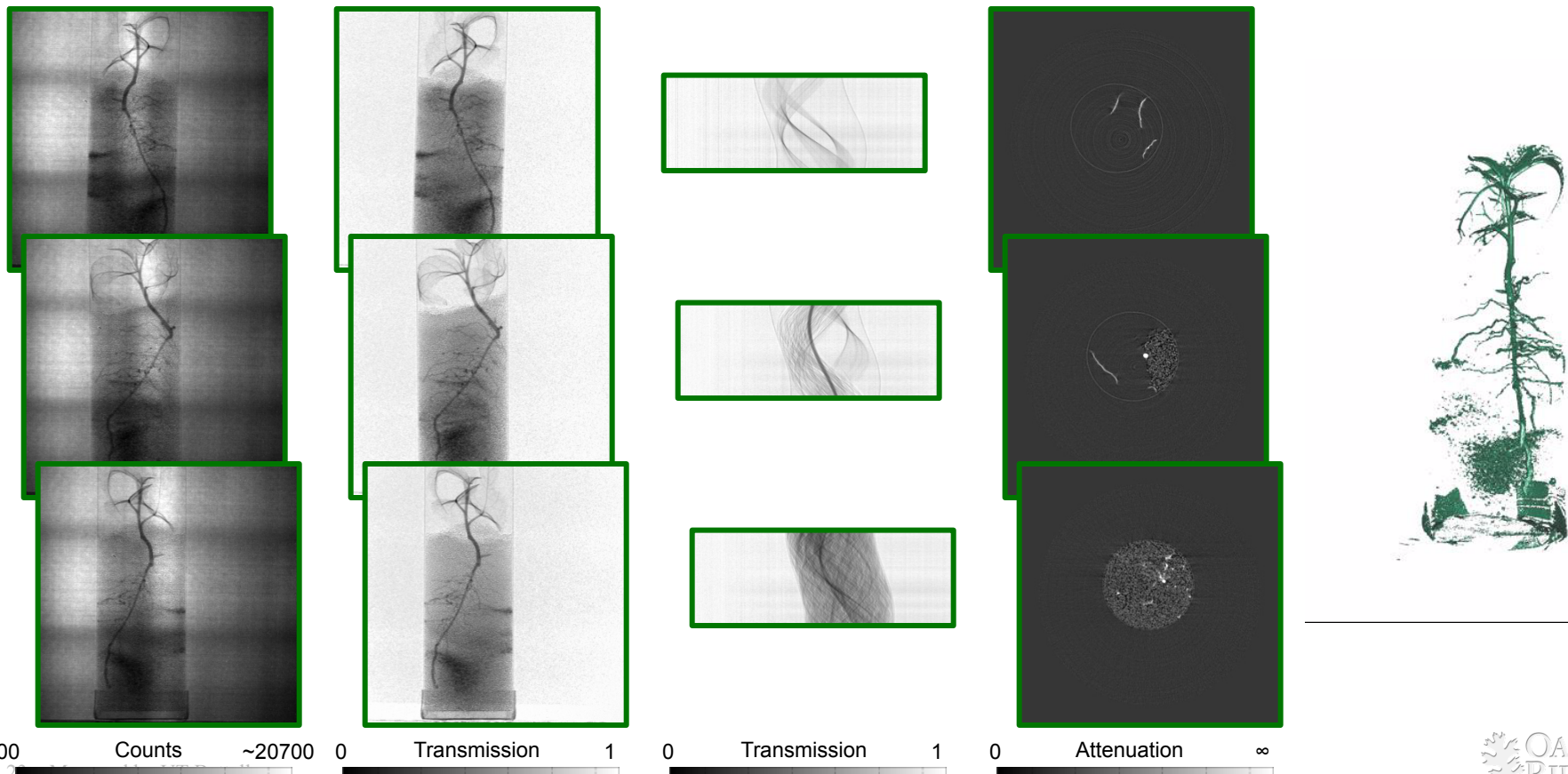


Computed/Computerized Tomography (CT)

- **Several techniques:**
 - **Filtered Back Projection**
 - Radon transform
 - Works well with high signal to noise ratio measurements
 - Easy-to-use commercial, semi-automated software available
 - Quick
 - **Iterative Reconstruction**
 - Direct approach
 - Less artifacts
 - Can reconstruct incomplete data
 - High computation time

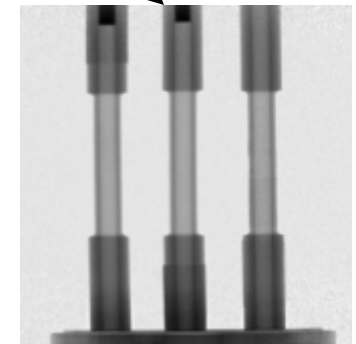
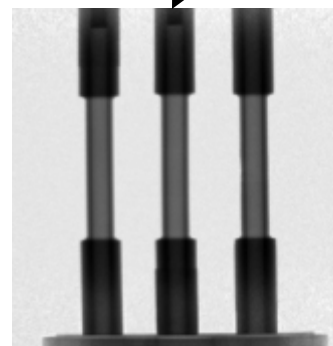
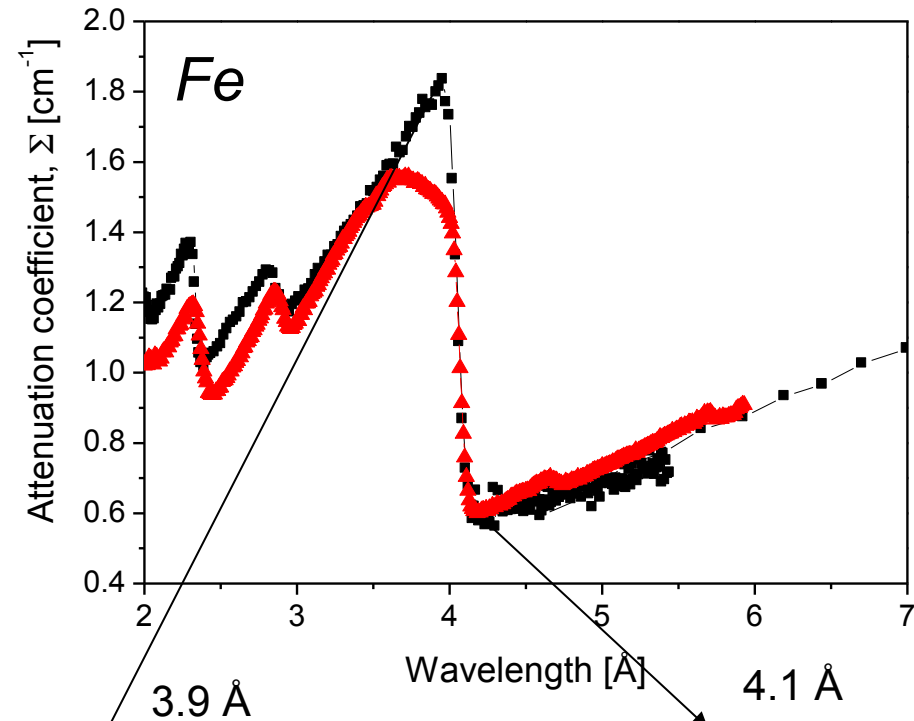
Computed/Computerized Tomography (FBP)

– Filtered back projection method



Bragg Edge Imaging

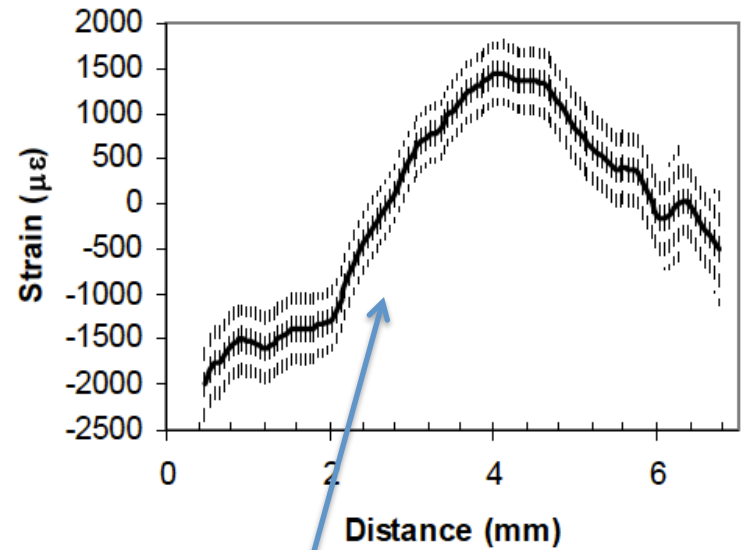
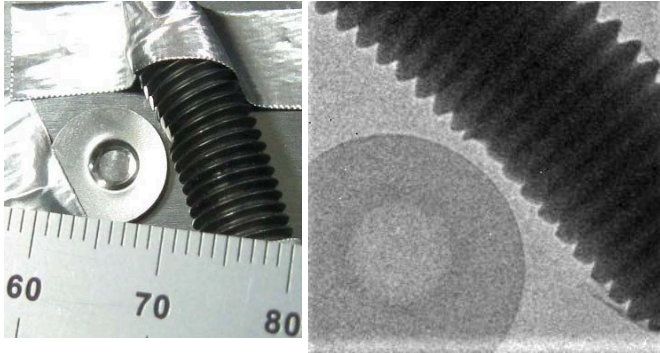
- **At reactors:**
 - monochromatic beams
 - Scintillator-based detection adequate
- **At spallation sources:**
 - Time-stamping of neutrons
 - Pixelated detectors such as MCPs required for time measurements



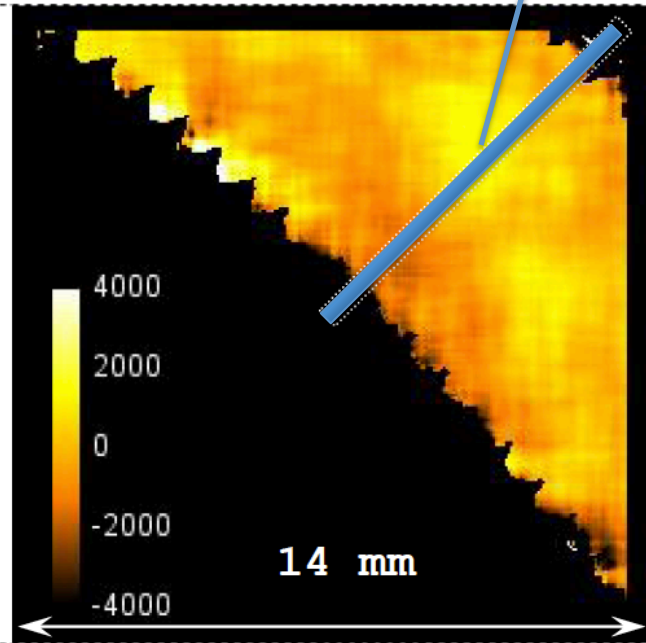
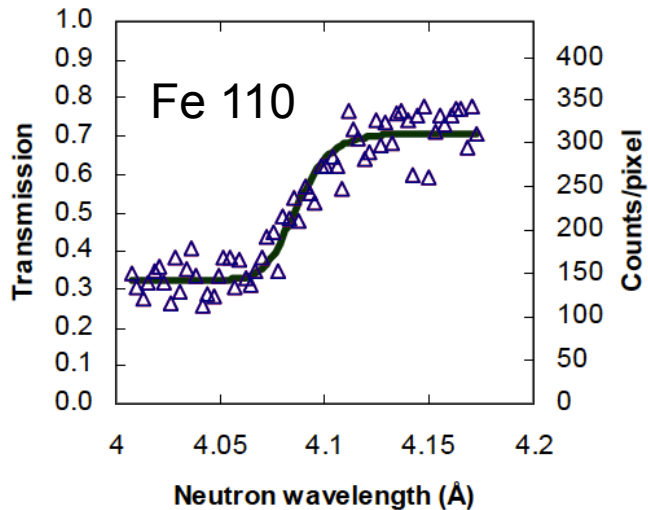
Courtesy of Prof. D. Penumadu, UTK and N. Kardjilov, HZB

Bragg Edge Imaging

- Strain mapping of steel screw



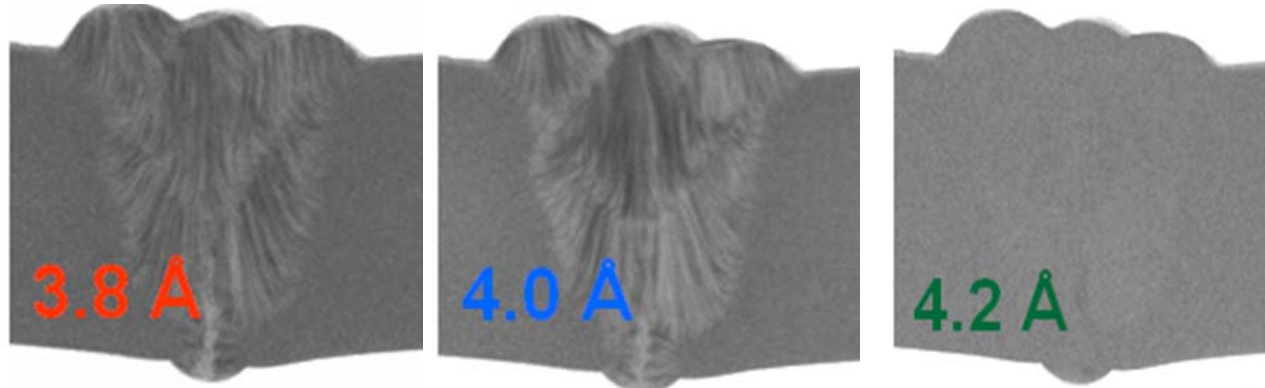
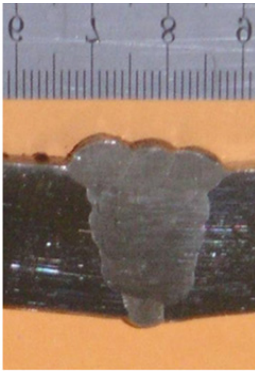
5 min exposure, 1 μs time res.



Strain map image of the steel screw. Strain values in μstrain

Bragg Edge Imaging

- Texture mapping



Bragg reflected neutrons result in narrow dips in the actual transmission at precise wavelengths specified by Bragg's law:

$$\lambda_{hkl} = 2d_{hkl} \sin\theta_{hkl}$$

where d_{hkl} is the interplanar distance for the (hkl) planes and θ_{hkl} are the Bragg angles θ_{hkl} depends on the relative orientation of the crystal lattice to the neutron beam.

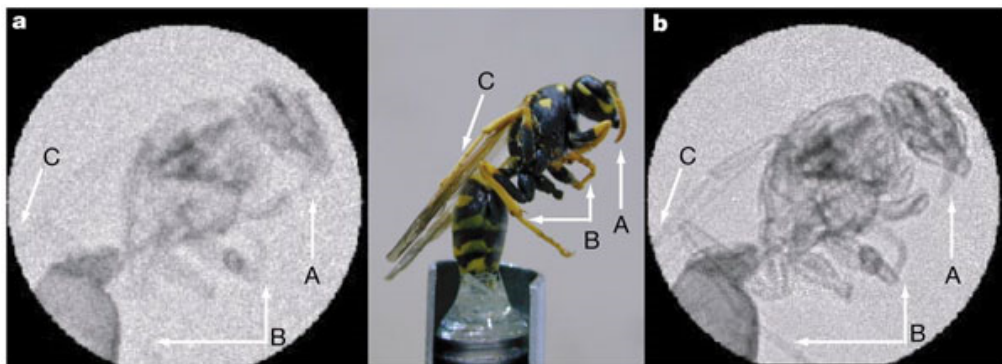
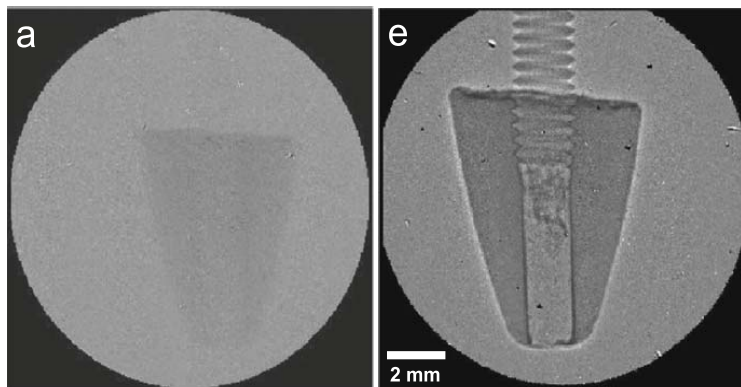
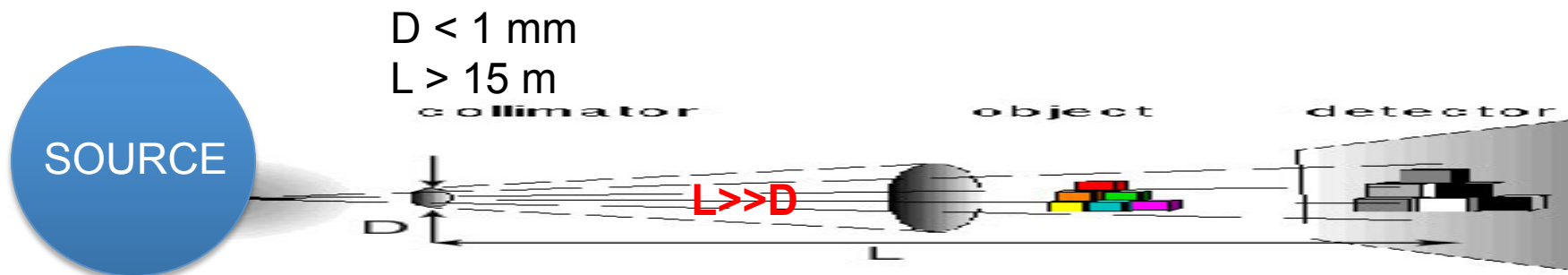
At λ_{hkl} , creation of map of the number of crystals having any of their (hkl) directions making an angle, β_{hkl} , with the incident beam given by:

$$\beta_{hkl} = (\pi/2) - \arcsin(\lambda_{hkl} / 2d_{hkl})$$

Kockelmann et al., NIM A, Vol. 578 (2007) 421.

Propagation-based Neutron Phase Imaging

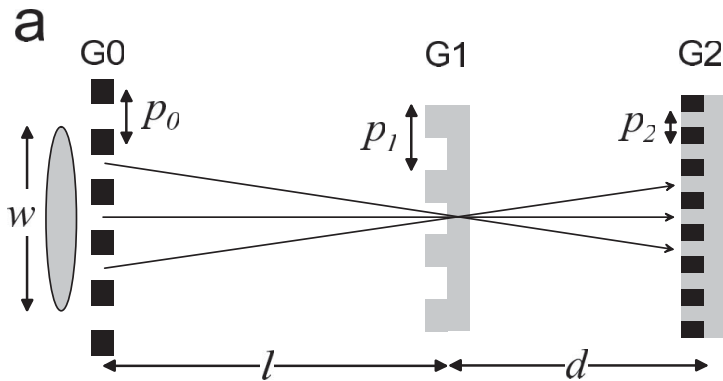
- Source needs to be spatially coherent (i.e. small pinhole and long pinhole-detector distances)
- Flux is low (up to 98% of flux is sacrificed, several hours to days for one radiograph)



(a) Neutron attenuation radiograph (e) and phase contrast radiograph of a lead sinker mounted on an Al screw. [B. Schillinger et al., *Mat. Trans. Proc.* (2006) 61]

(a) Neutron attenuation radiograph (b) photograph and (c) phase contrast radiograph of a yellow jacket wasp. [B. E. Allman et al., *Nature* 408 (2000) 158]

Phase Radiography using Grating Interferometry

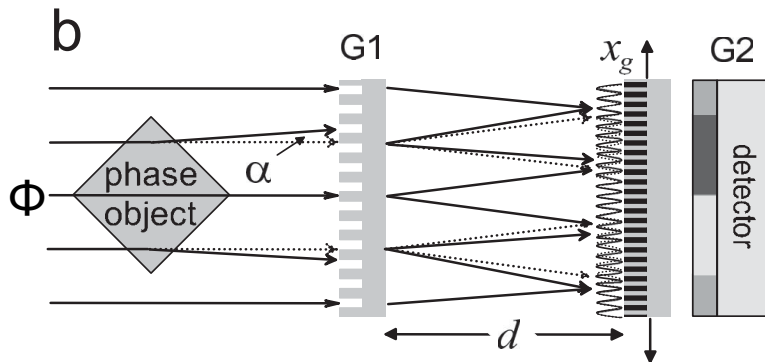


- G0 creates array of coherent sources from source w
- G1 creates diffraction patterns for each source which overlap if

$$p_0 = p_2 \frac{l}{d}$$

- Diffraction pattern has maximum contrast when d is a integer multiple of the Talbot length, L_T

$$L_T = \frac{p_1^2}{\lambda}$$



- Phase object cause distortion of diffraction pattern (or phase shift of incident wave Φ)
- Measure diffraction pattern by translating G2

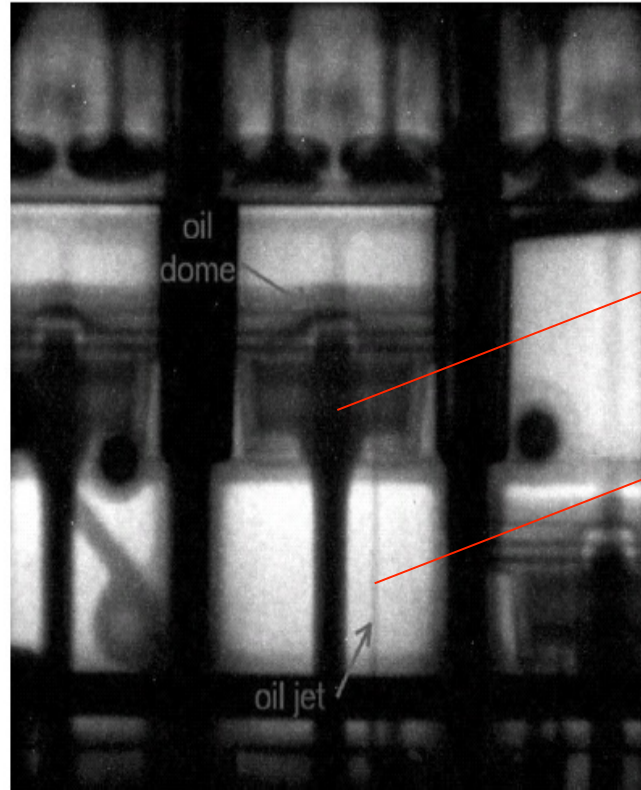
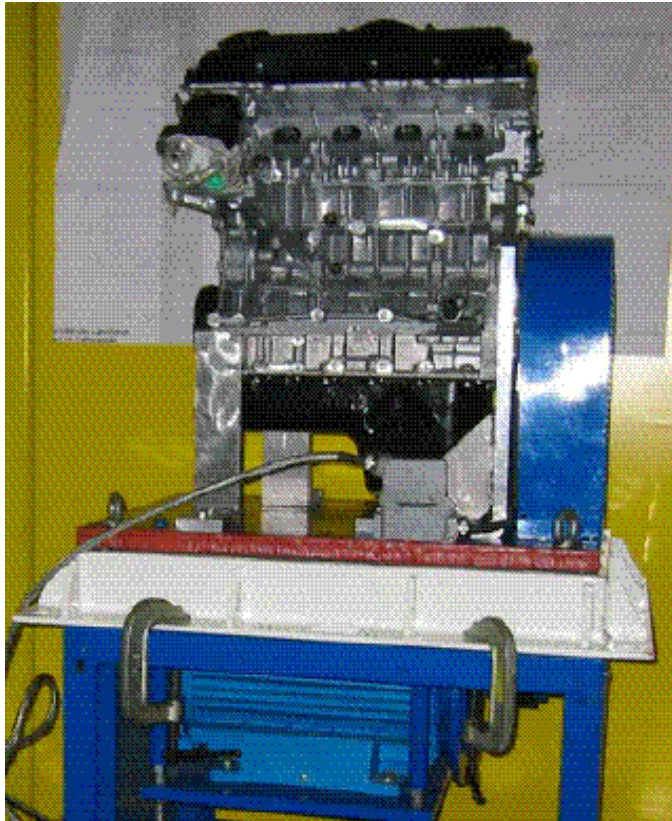
G0: (source) absorption grating, period p_0
 G1: phase grating, period p_1
 G2: (analyzer) absorption grating, period p_2

[Pfeiffer et al., **PRL**. 96 (2006) 215505]

$$p_0 \sim 1 \text{ mm}, p_1 \sim 10 \mu\text{m}, p_2 \sim 5 \mu\text{m}, l \sim 5 \text{ m}, d \sim 20 \text{ mm}$$

Stroboscopic imaging

- Makes a cyclically moving object appear to be slow moving
- Pulsed sources are by definition stroboscopic neutron sources



Oil spreading
into bottom of
piston

Oil jet
ejected into
bottom of
piston

Stroboscopic imaging:
150 exposures, 200 ms
each, 24 cm x 24 cm
field of view

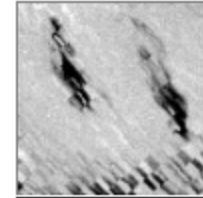
BMW engine, NEUTROGRAPH, ILL, France

Schillinger et al., NIM A **542** (2005) 142.

Applications at a glance

- Archeology
- Bio-medical
- Botany
- Contraband
- Cultural Heritage
- Energy
- Engineering/Materials Science
- Forensic Science
- Geology/Earth Sciences
- Homeland Security
- Paleontology
- Quality Assurance

Visualization of water transport in artificial soil sedimentation (20 s frame, 25 x 25 cm²)



<http://neutra.web.psi.ch/gallery/animations.html>

Radiography of a dry monkey skull



<http://neutra.web.psi.ch/gallery/biological.html>

Fluid flow in porous media



Develop quantitative imaging techniques using neutrons to accurately measure the 2-D distribution of water/oil in porous media

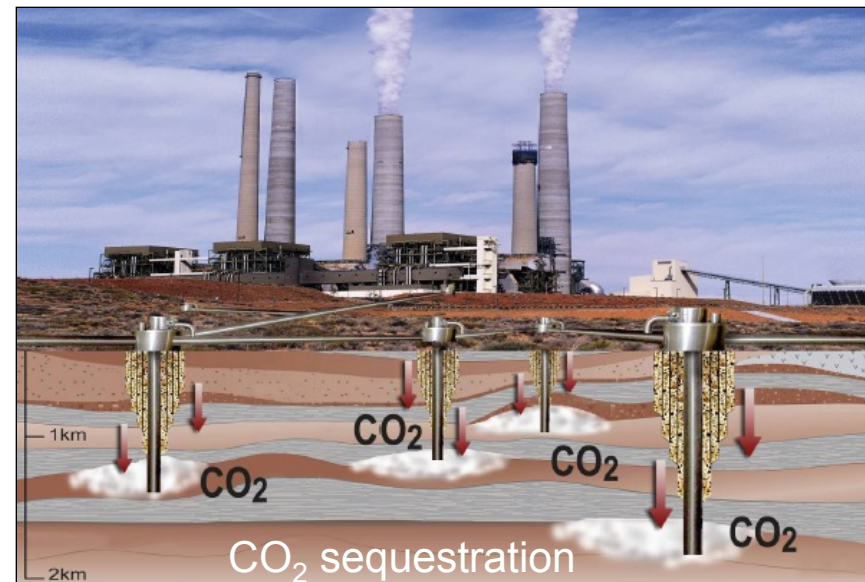
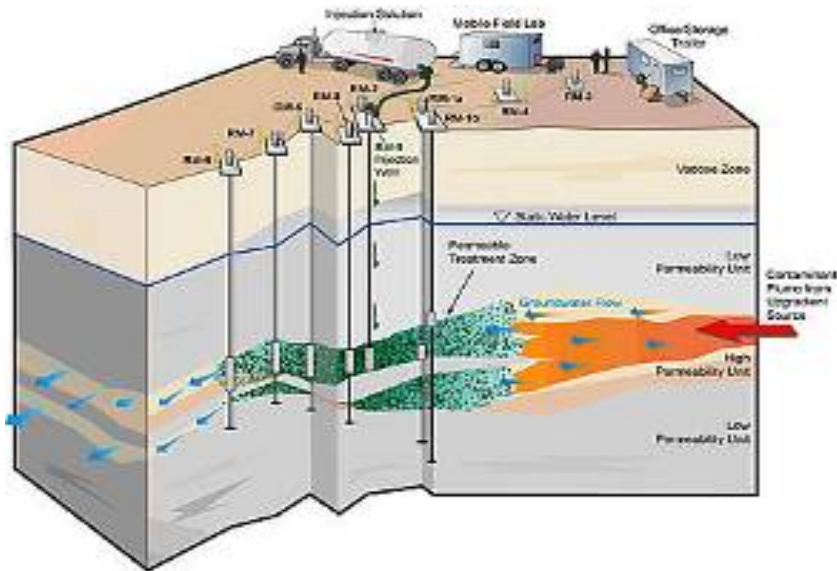
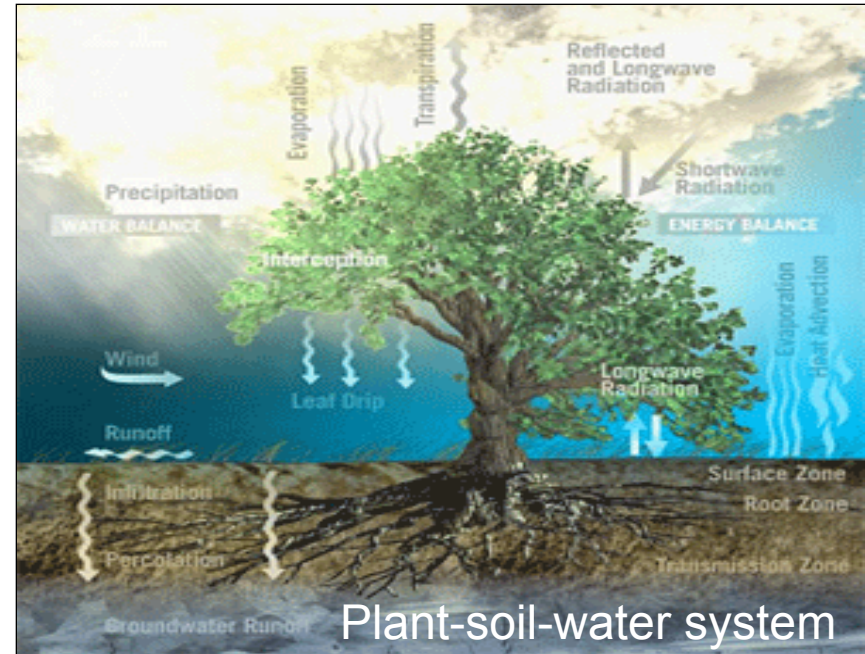
Evaluate analytical models for predicting water/oil flow in porous media

Provide input parameters for numerical modeling

In collaboration with Prof. Perfect and Dr. Cheng at UTK, Prof. Horita at Texas Tech. and Dr. Warren at ORNL.

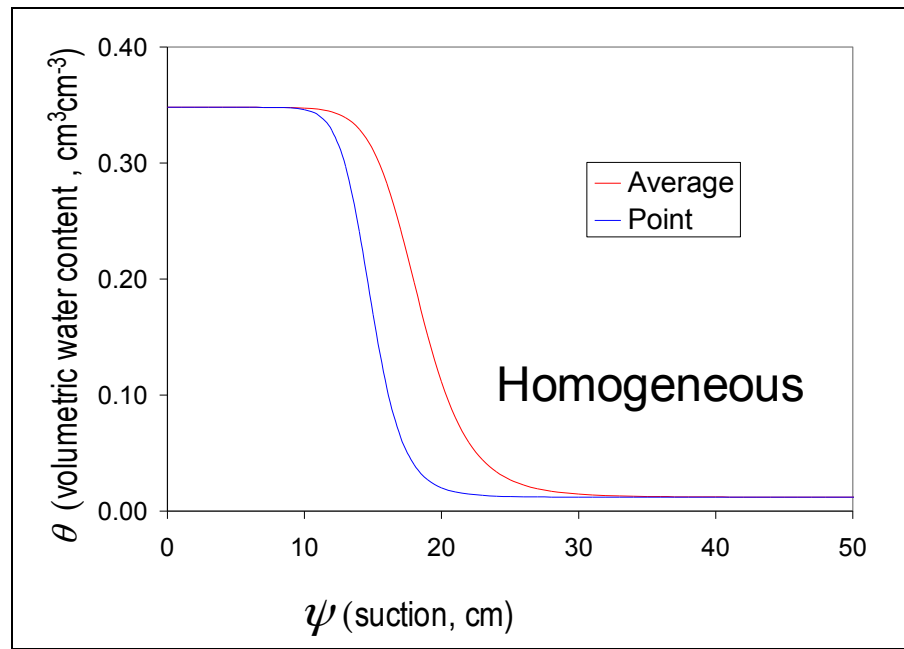
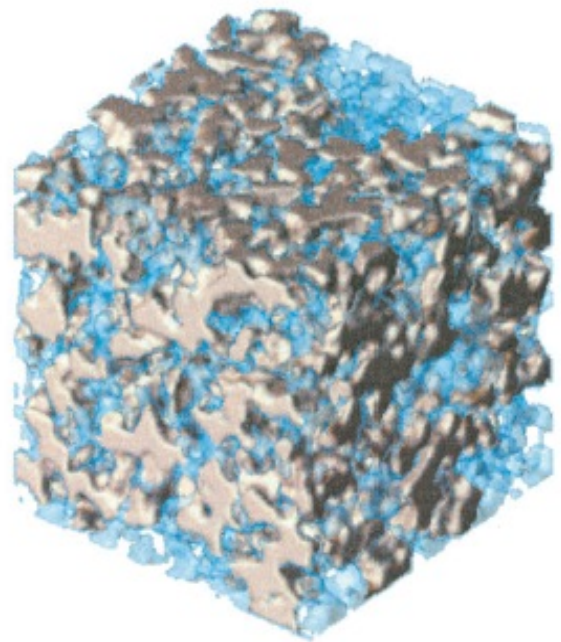
Significance

- Water in porous media
 - agricultural crop production
 - infiltration & aquifer recharge
 - remediation of contaminated soils
 - subsurface carbon sequestration
 - enhanced oil recovery

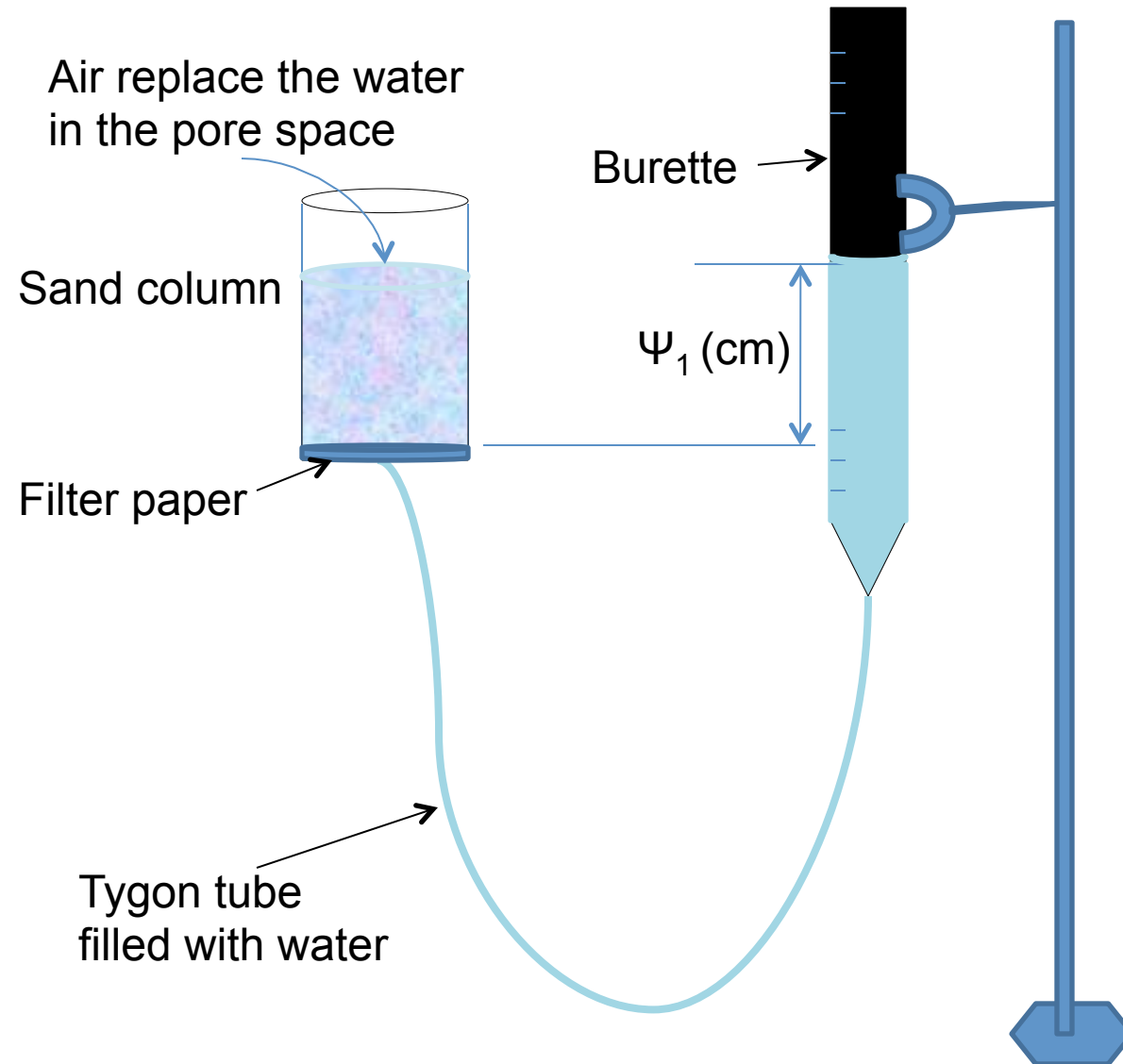


Water in Porous Media

- Traditionally determined using “black box” methods:
 - hanging water column & pressure plates
- Water retention curve: suction (ψ) imposed at a particular point in the porous medium & corresponding average water contents (θ_{avg})
- **Point function, $\theta(\psi)$, curve** needed for modeling flow & transport in porous media
- $\theta(\psi)$ extracted by modeling $\theta_{avg}(\psi)$
 - TrueCell (analytical) and STOMP (numerical) models
- Neutron imaging allows us to “see” into the black box & measure $\theta(\psi)$ directly

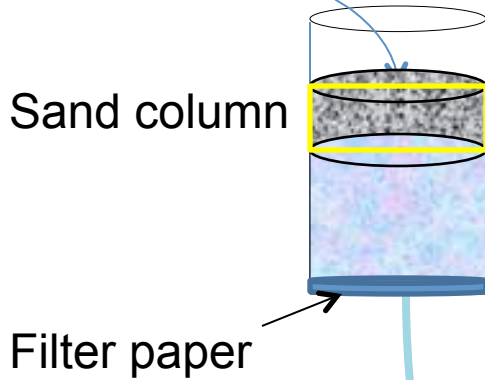


Hanging water column, $\theta_{avg}(\psi)$



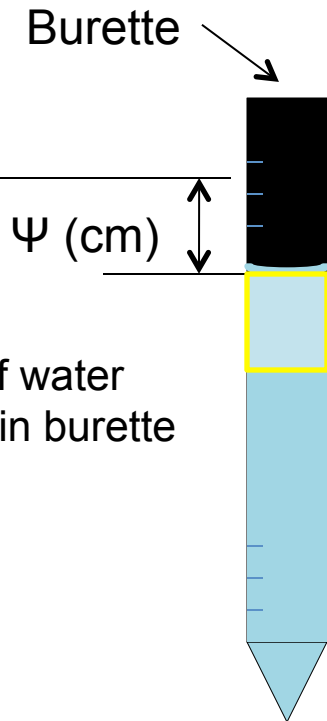
Hanging water column, $\theta_{avg}(\psi)$

Air replace the water in the pore space



Volume of water drained from sand column

= Volume of water collected in burette



Drying Process

Burette: Down



- Let the system equilibrate
- Record the water level and height

Average water content = volume of water retained in sand column/total volume of sand column

Tygon tube filled with water

Hanging water column, $\theta_{avg}(\psi)$

Air replace the water in the pore space

Soil column

Burette

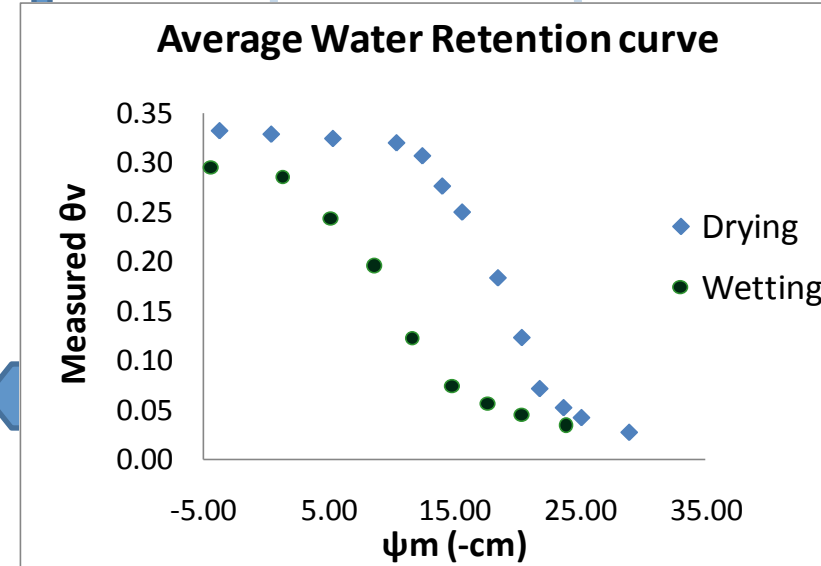
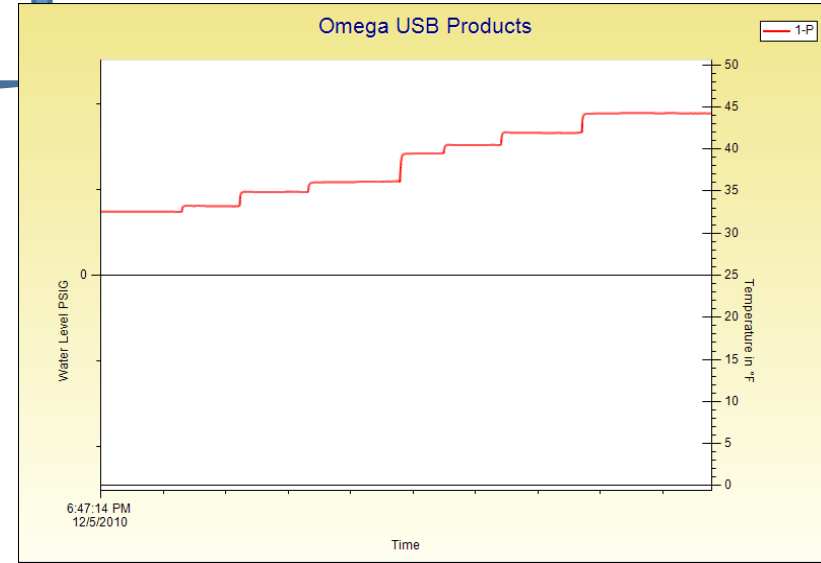
Ψ_1 (cm)

Filter paper

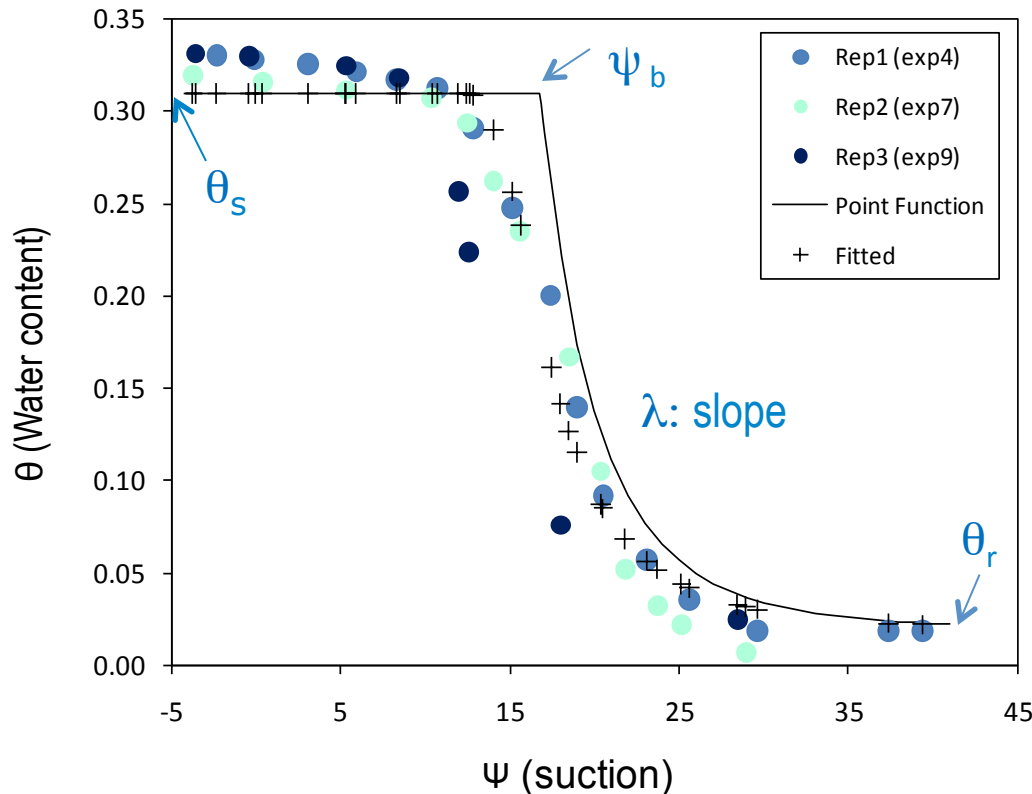
Tygon tube filled with water

Drying Process

Wetting Process



Point Water Retention Function: hanging water column

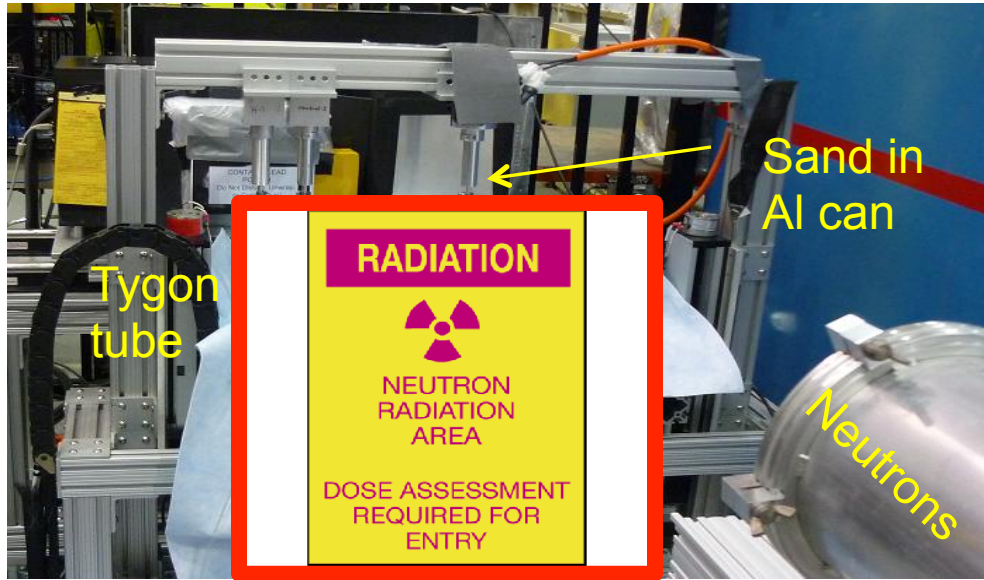


Brooks and Corey Parameters

- θ_r = residual water content ($\text{cm}^3\text{cm}^{-3}$)
- θ_s = saturated water content ($\text{cm}^3\text{cm}^{-3}$)
- ψ_b = air entry value (cm)
- λ = pore-size distribution index

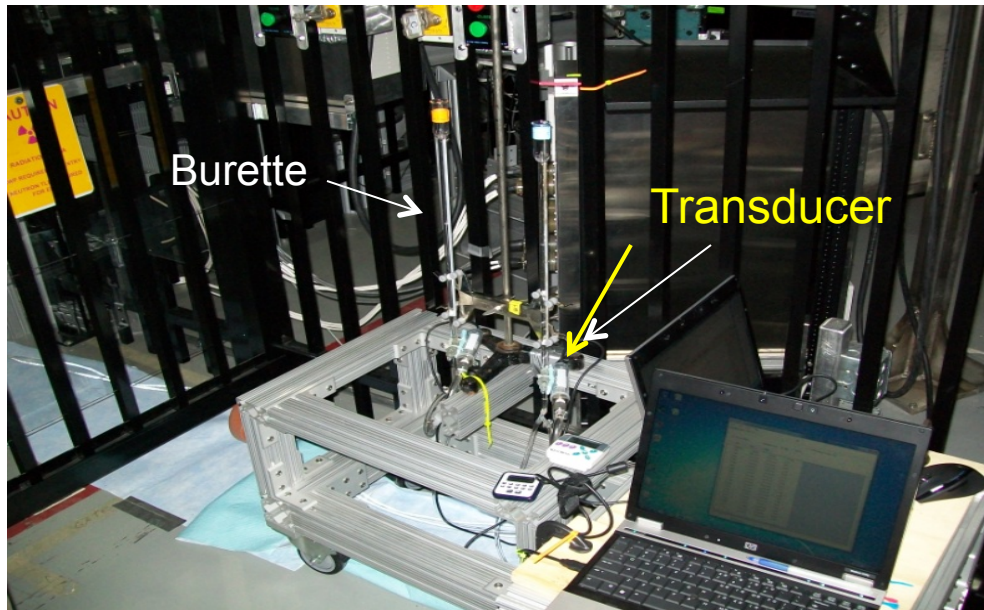
➤ Point water retention function is extracted from the average water retention curve determined by hanging water column using TrueCell inverse modeling procedure

Hanging water column set up for neutron imaging at CG-1D



Sample

- Flint #13 sand and Handford sediment
- Al cylinder 2.6 cm ID, 4 to 6cm height sand column
- Median particle size: 0.56mm, Particle density: 2.65 g/cm^{-3}

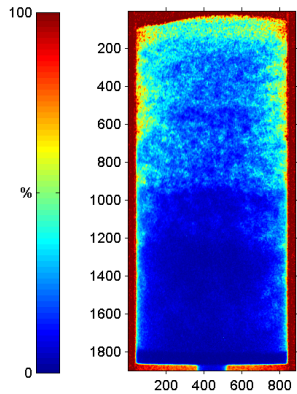


Procedure

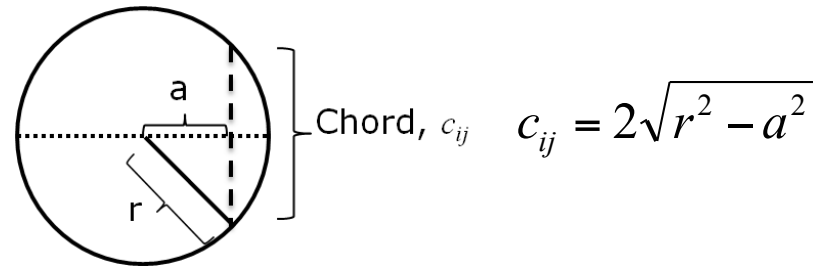
- Hanging water column set up
- Placed in path of incident neutron beam
- Various suction applied using hanging water column
- Radiography (2-D) Images during drainage and rewetting process with 60 second exposure time

Image Analysis for Sand in Cylindrical AI chamber

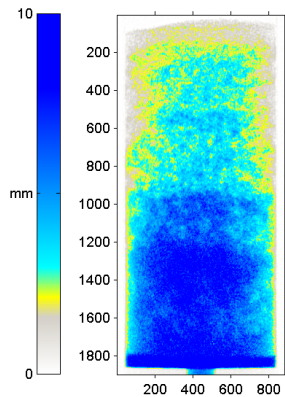
- Steps for 2-D image analysis to quantify volumetric water content in sand column



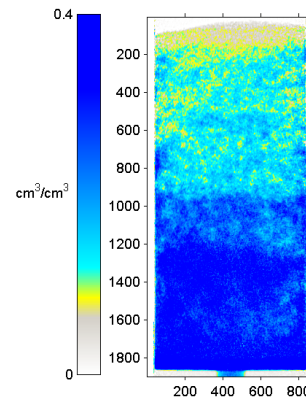
$$I_n = \frac{\text{Raw Image} - \text{Dark Field}}{\text{Dry Image} - \text{Dark Field}}$$



$$c_{ij} = 2\sqrt{r^2 - a^2}$$

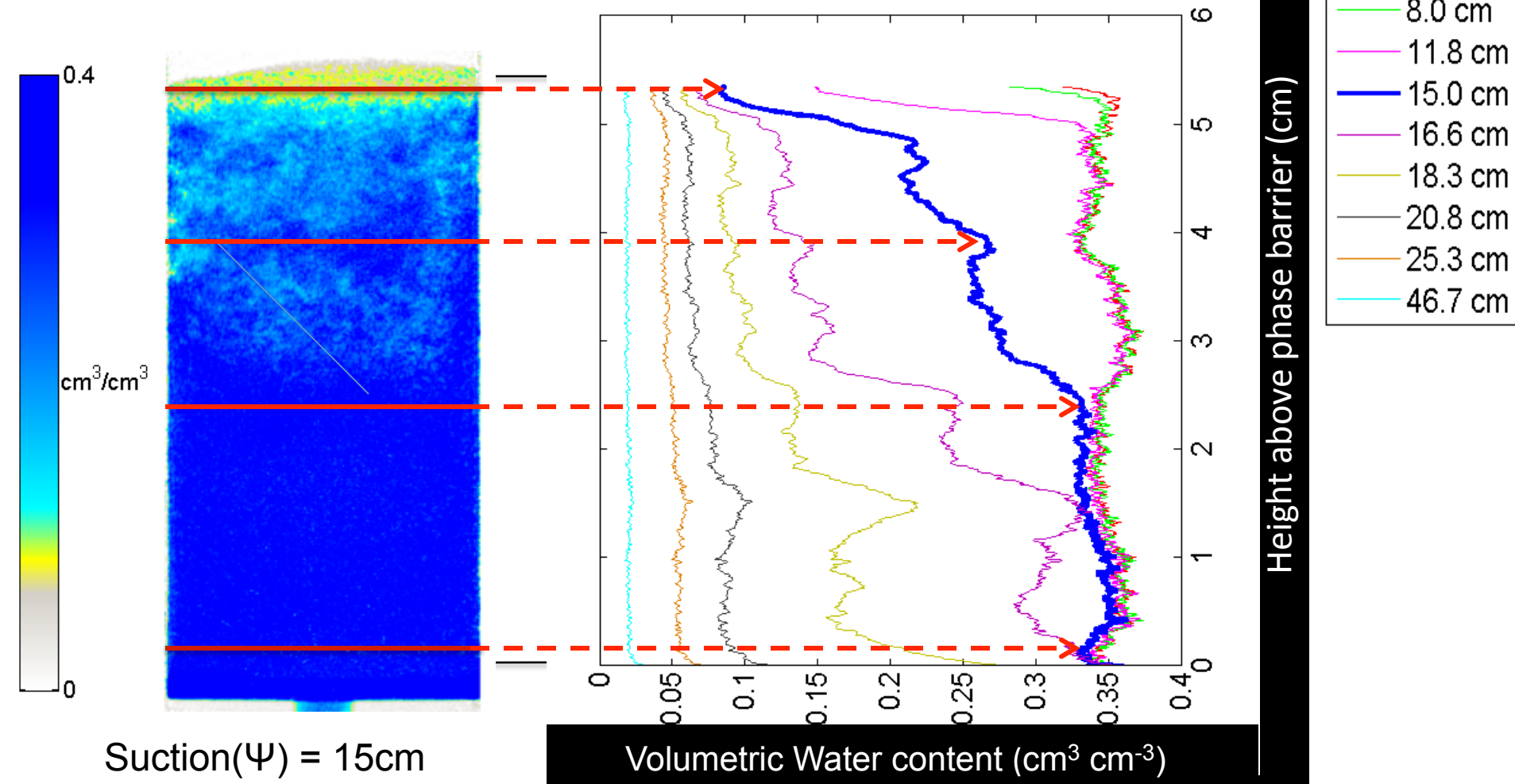


$$\tau_{ij} = -\frac{\mu}{2\beta} \pm \sqrt{\left(\frac{\mu}{2\beta}\right)^2 - \frac{1}{\beta} \log(I_n(i, j))}$$

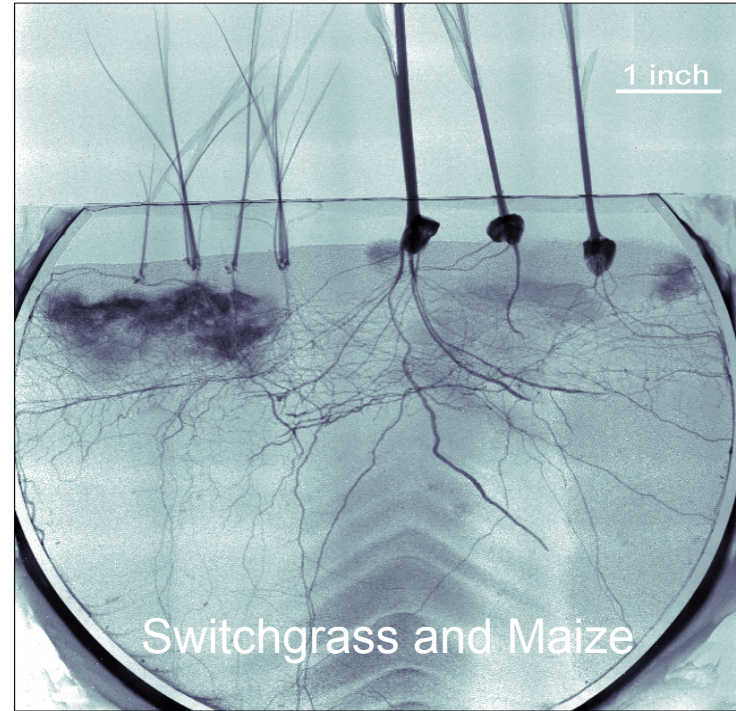
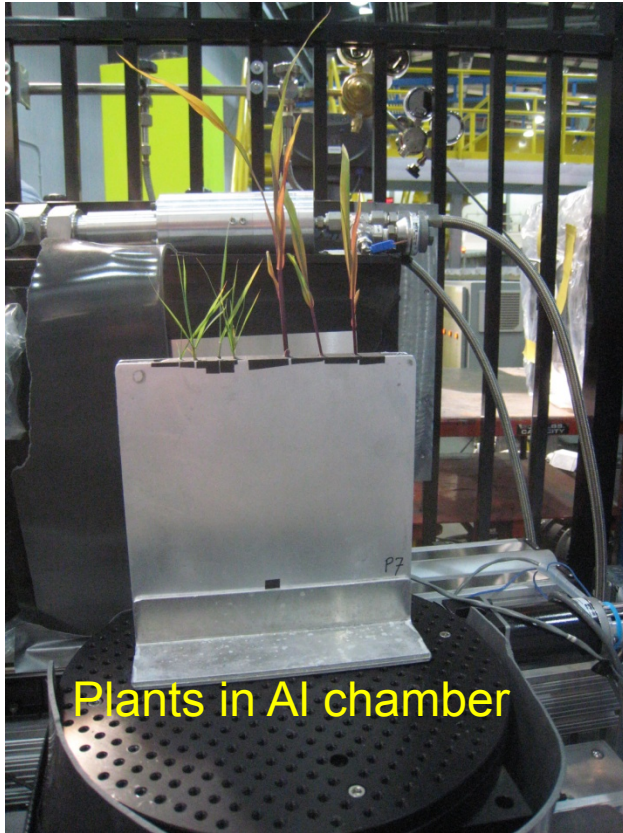


$$\theta_{ij} = \frac{\tau_{ij}}{c_{ij}} \times \frac{\text{pixel area}}{\text{pixel area}}$$

Quantification of Water Content as a Function of Height by Neutron Radiography



Neutron Radiography of Roots at CG1-D



- Water injected into root zone at base
- Unidentified endophyte (symbiotic) or decomposer fungi visible near roots of switchgrass (left), revealing substantial hydration of the rhizosphere
- Both fine and coarse roots are readily visible

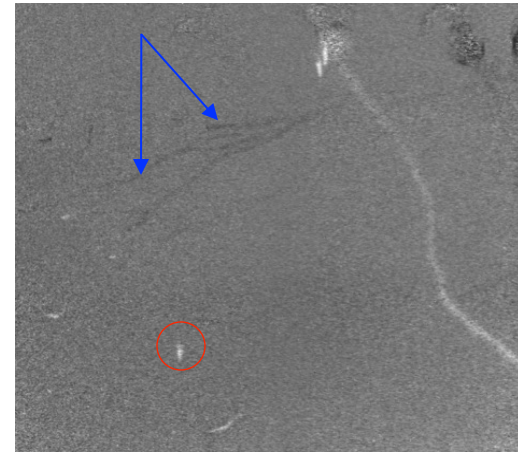
Changes in Soil and Root Water Content using Neutron Radiography



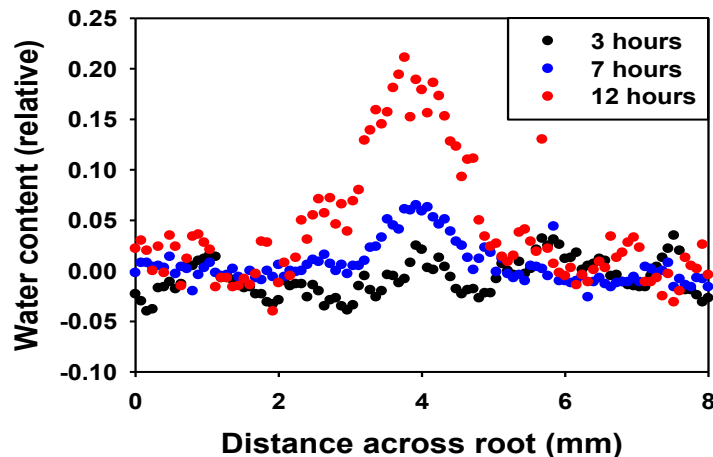
t = 0 h



t = 12 h



t = 12/t = 0

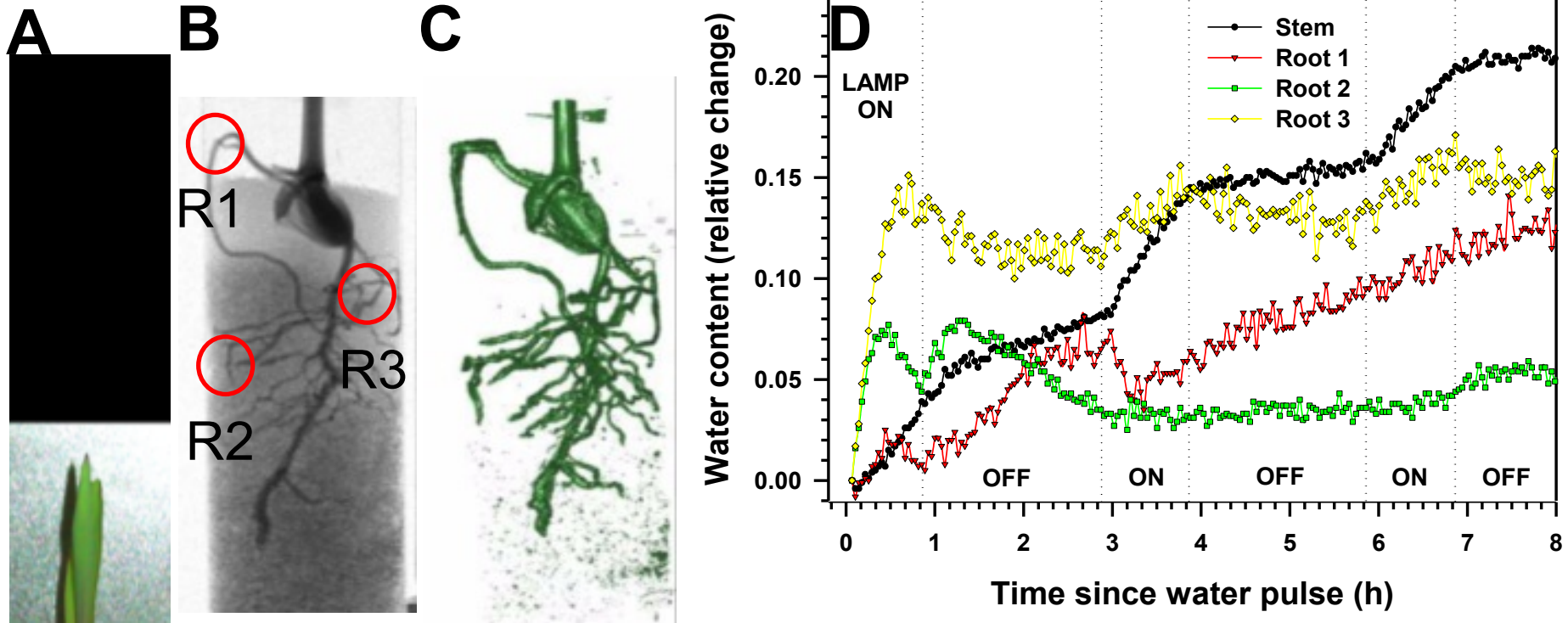


Top – More water showing up based on division (white areas)

Blue arrows show where water was removed from the system.

Left – increase in water content or root or rhizosphere due to root growth or root water efflux

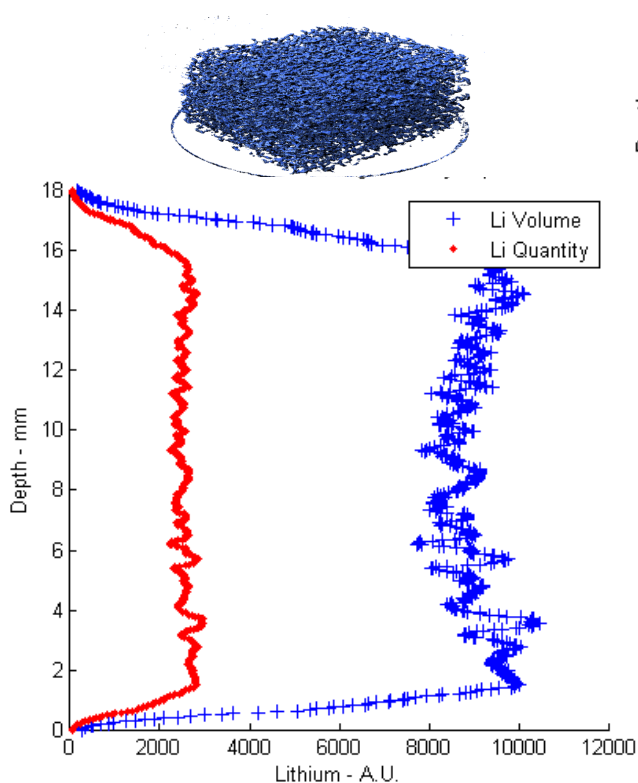
Water Uptake by Roots and Stem



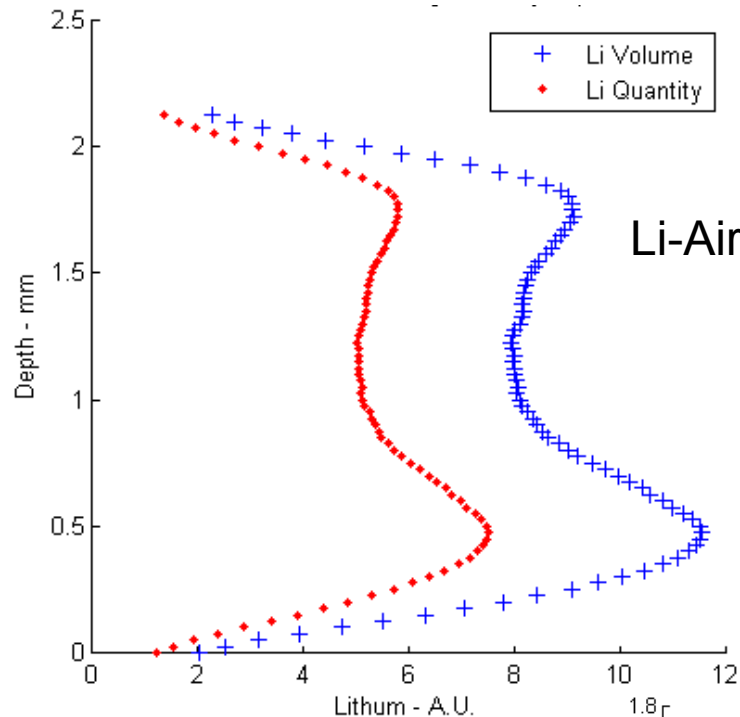
10-d old maize seedling (A) aluminum sample chamber; (B) neutron radiograph at $\sim 70 \mu\text{m}$ pixel resolution illustrating roots distribution (0.2-1.6 mm); (C) 3D tomographic reconstruction; (D) Timing of water uptake by plant components highlighted in (B) illustrating impact of solar radiation on rate of water flux in stem and $\sim 0.5 \text{ mm}$ first and second order roots.

➤ This study provides direct evidence for root-mediated hydraulic redistribution of soil water to rehydrate drier roots

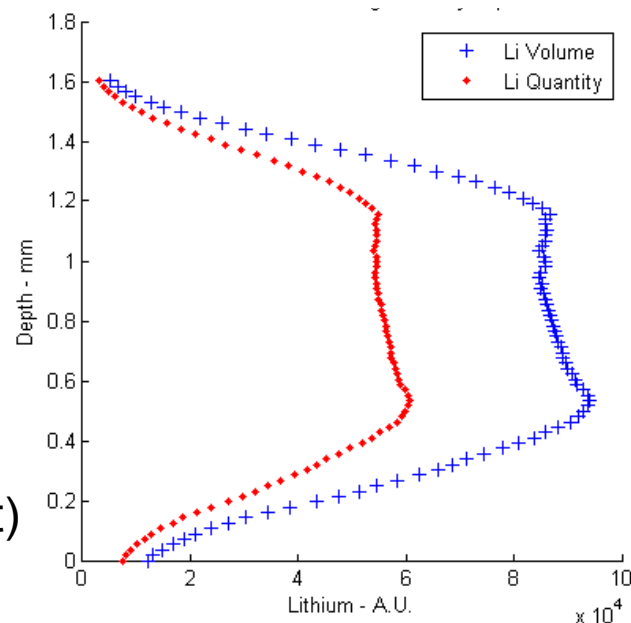
Comparison of Li Distribution as a function of depth of battery



Control



Li-Air (no catalyst)

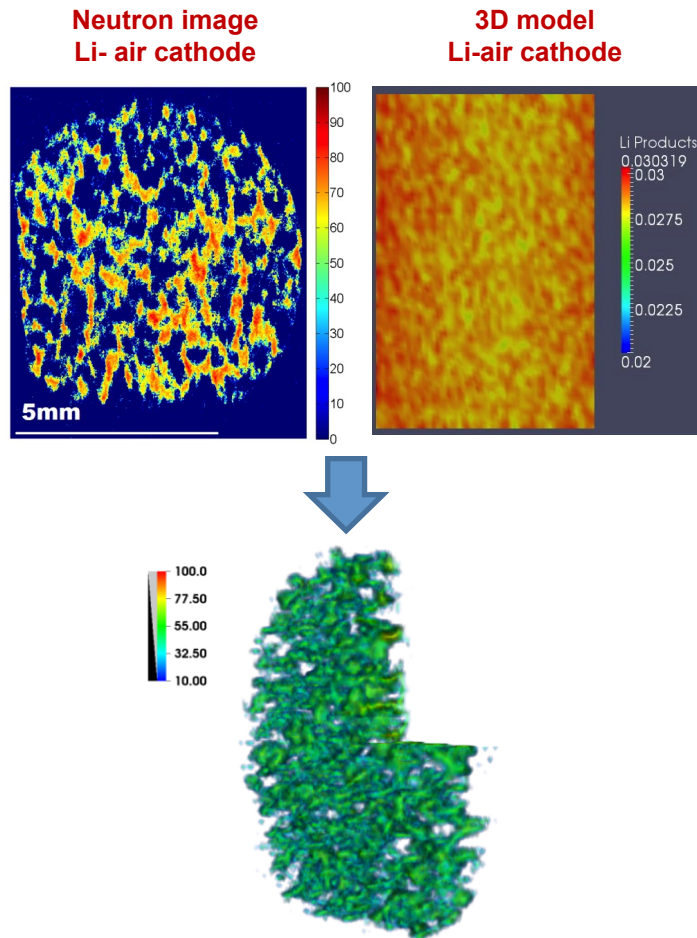


Li-Air (with catalyst)

Nanda et al., Journal of Physical Chemistry C, 2012.

Neutron imaging provides the basis for developing models

Non-uniform lithium distribution may limit rechargeability



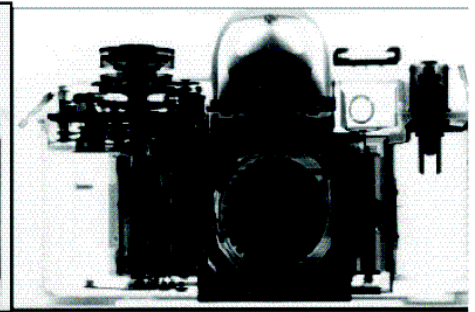
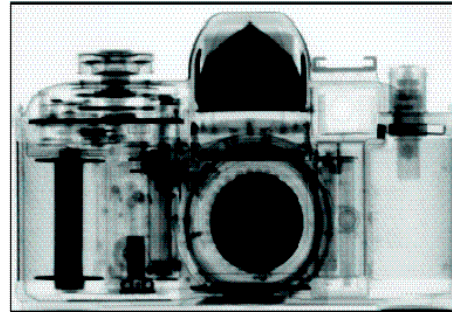
- Reaction phase 3 dimensional modeling was used to predict results and compare with measurements
- Spatiotemporal reaction phase three-dimensional modeling of the electrodes also predicted a non-uniform lithium product distribution, confirming the neutron imaging result.
- Need to match resolution of neutron imaging capabilities to further improve feedback to modeling tools

Image produced by neutron-computed tomography.

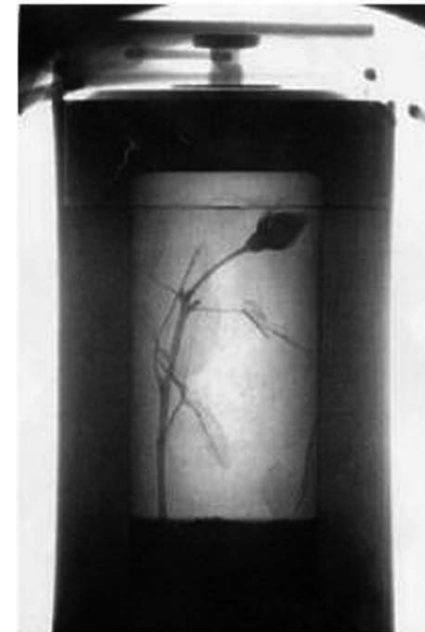
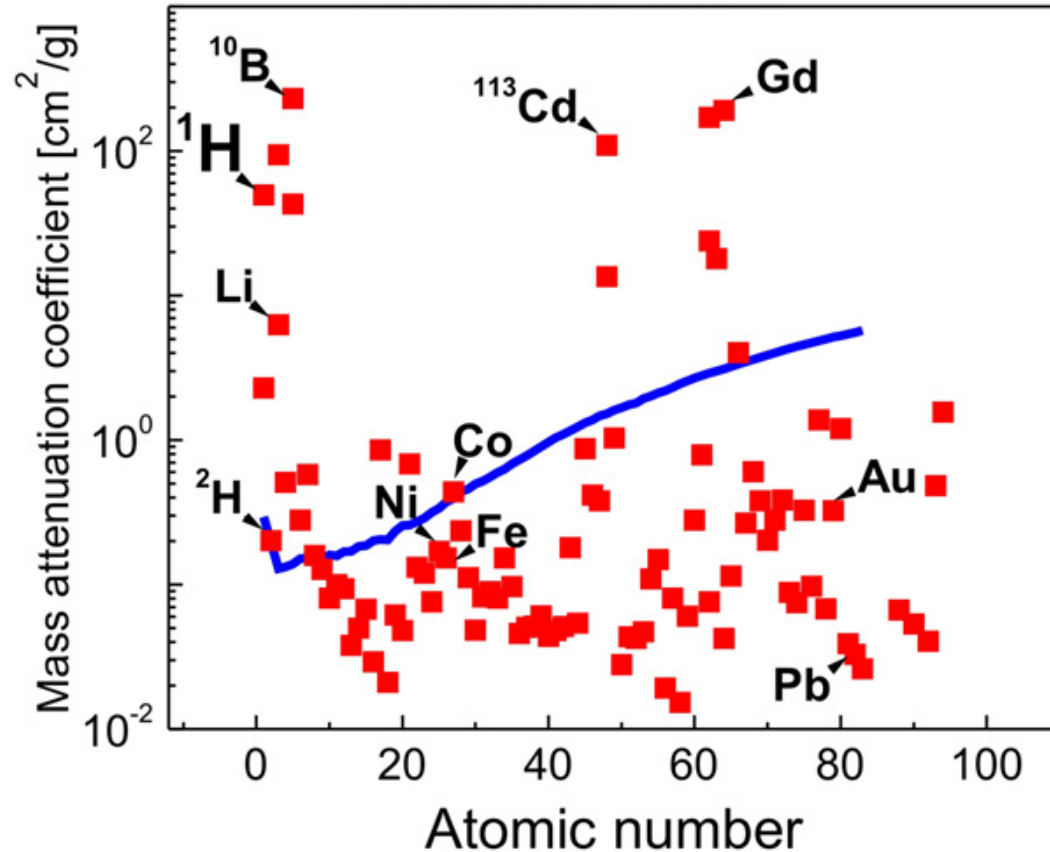
Neutron sensitivity

Neutron Radiograph of camera

X-ray Radiograph of camera



— X-rays (100 keV)
 ■ Thermal neutrons



Neutron Radiograph of Rose in Lead Flask

[M. Strobl et al., *J. Phys. D: Appl. Phys.* **42** (2009) 243001]

Courtesy of E. Lehmann, PSI

Thank you

Courtesy of
Krysta Ryzewski, Wayne University
Susan Herringer, Brian Sheldon,
Brown University

